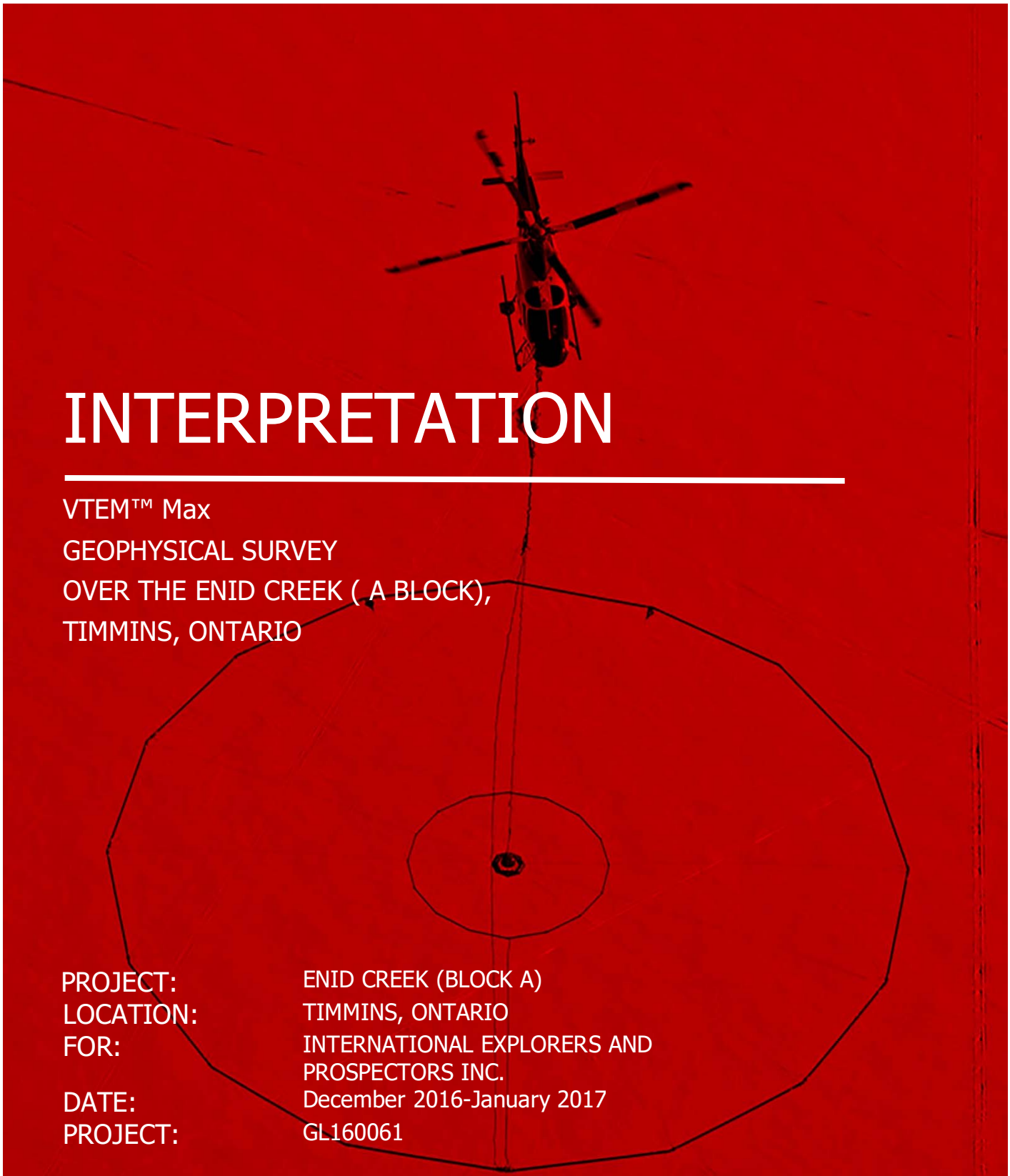

INTERPRETATION

VTEM™ Max
GEOPHYSICAL SURVEY
OVER THE ENID CREEK (A BLOCK),
TIMMINS, ONTARIO

PROJECT:	ENID CREEK (BLOCK A)
LOCATION:	TIMMINS, ONTARIO
FOR:	INTERNATIONAL EXPLORERS AND PROSPECTORS INC.
DATE:	December 2016-January 2017
PROJECT:	GL160061

Geotech Ltd.
245 Industrial Parkway North
Aurora, ON Canada L4G 4C4

Tel: +1 905 841 5004
Web: www.geotech.ca
Email: info@geotech.ca

GEOTECH
AIRBORNE GEOPHYSICAL SURVEYS

TABLE OF CONTENTS

LIST OF FIGURES

APPENDICES

EXECUTIVE SUMMARY

Between December 3rd, 2016 and January 31st, 2017 GEOTECH LTD conducted a helicopter-borne geophysical survey using a VTEM™ max system and a high sensitivity magnetometer over the A Block (Enid Creek) located 27 km west of Timmins, in Ontario. In total, 96 line kilometers of airborne EM and magnetic data acquisition were collected over the survey area, using an Aerospatiale A-Star B3 helicopter, operated by Geotech Aviation Ltd. The traverse lines were flown in the NS direction at azimuth of 0°-180° NE and were spaced at 100 m apart. The tie lines were flown in the orthogonal direction (east-west) and were spaced at 1000 m apart. The helicopter was flying at a mean speed of 80 km/h and at average altitude of 96 m above ground. The average ground clearance of the EM transmitter-receiver system was 49 m.

From historic work, the property is known to include copper-nickel-sulphide mineralization hosted by gabbroic intrusions. Ground and airborne geophysical surveys, surface geological mapping and diamond drilling programs were executed on the property by various companies since the mid-1960s.

The aim of the recent airborne geophysical survey executed with VTEM system was to delineate new potential areas for further exploration of copper-nickel-sulphide mineralization in this property. The acquired magnetic data were transformed into various maps and inverted in 3 dimensions to provide a 3D distribution of the magnetic susceptibility and magnetization vector amplitude of the subsurface area. The magnetic data interpretation resulted into a new detailed structural analysis that helped map numerous mafic dikes, faults and outlines of magnetic structures. The EM data were analyzed and transformed into resistivity plan maps and sections and were inverted in 1D, 2.5 and 3D to characterize the rocks electrical properties of the subsurface area and to better define EM targets.

Based on the integrated EM and magnetic data interpretation and their inversion results, six (06) favourable targets for the exploration of nickel-sulphide mineralization were identified and delineated. Four targets are associated with zones of elevated conductivity and elevated magnetization and two targets are associated with linear conductors occurring within moderately magnetic zones.

1. INTRODUCTION

This report summarizes the interpretation results of a helicopter-borne survey carried out by Geotech Ltd using a VTEM™ Max system over the A BLOCK (Enid Creek) located 27 km NW of Timmins, Ontario. The helicopter-borne geophysical VTEM™ Max system is consisting of a concentric in-loop system (Transmitter/Receiver) using a large transmitter loop of 35 m in diameter. The system produces a peak dipole moment of 750,000 NIA allowing a great depth of investigation. The EM system was towed at a mean distance of 35 metres below the helicopter. The magnetometer, towed in a bird at 13 metres below the helicopter was a Geometrics high-resolution cesium magnetometer. Ancillary equipment consisted of GPS navigation instrumentation, a radar altimeter, a power line monitor and a base station magnetometer. The EM ground clearance of the EM transmitter/receiver system was 50 m in average. 96 line kilometres were flown along lines oriented in the north-south direction and spaced at 100 metres apart covering an area of approximately 8.5 km^2. Tie lines, flown in the orthogonal direction were spaced at 1,000 metres apart. More details about the survey specifications are included in the processing report (Geotech, 2017)

The acquired airborne magnetic and electromagnetic data with the VTEM™ max system were analyzed, interpreted and inverted in 1D, 2.5D and 3D. The data interpretation results have identified and delineated several potential targets for the exploration of Cu-Ni-sulphide mineralization within the survey area.

2. PROPERTY DESCRIPTION

The BLOCK A is located 27 kilometres northwest of Timmins, Ontario. Local relief is flat with mean elevation of 300 m above mean sea level. The main river, Enid Creek is located in the west side of the property. Access to the property from Timmins is via Highway 101, Highway 576 and Kamiskotia Forestry Road.

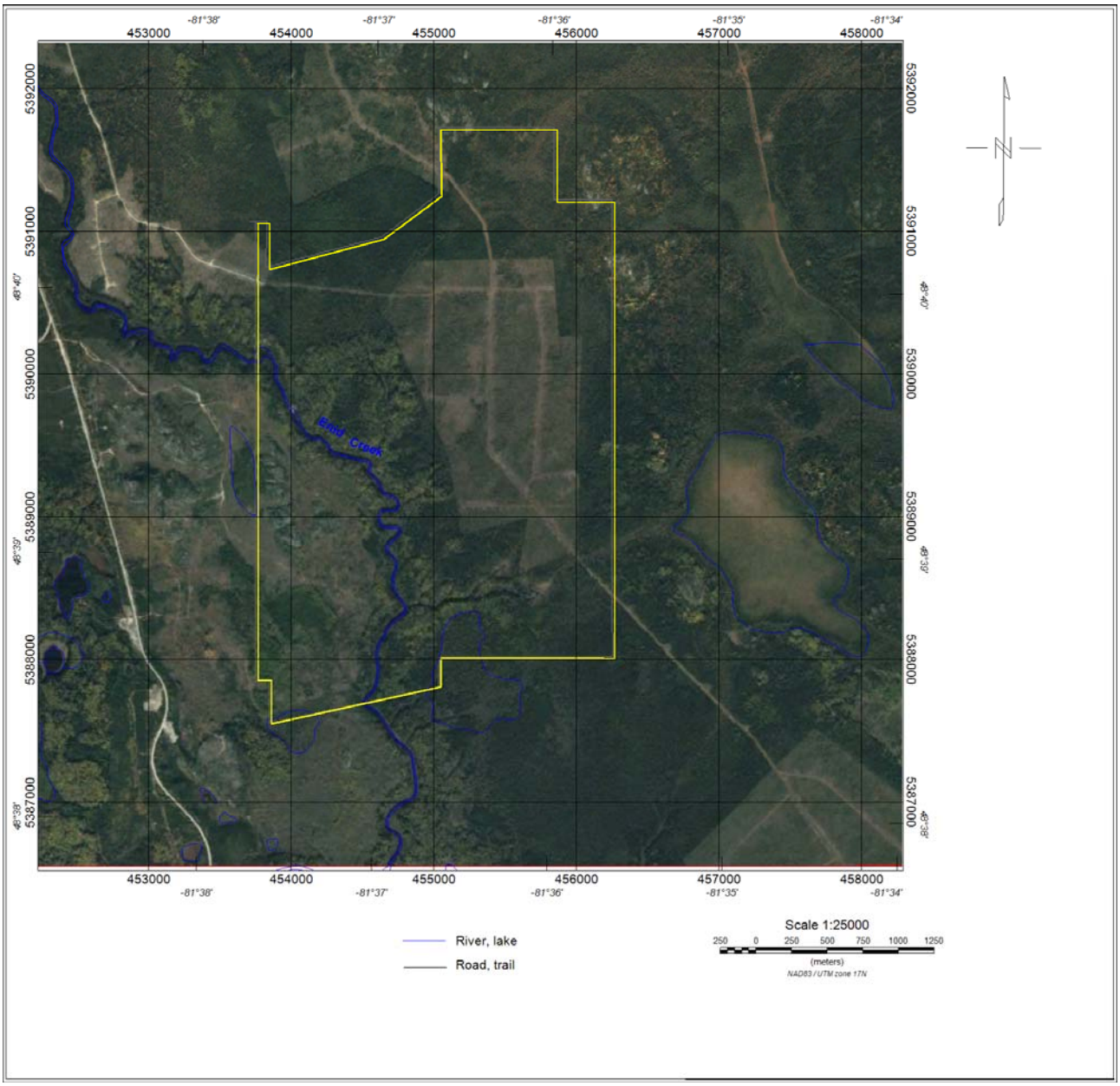

Figure 1: Location map of the BLOCK A in Google Earth. The VTEM survey outline is in yellow.

3. VTEM SURVEY SPECIFICATIONS

In total 96 line kilometers of VTEM and magnetic data acquisition were collected over the survey area, located 27 km northwest of Timmins, in Ontario using an Aerospatiale A-Star B3 helicopter, operated by Geotech Aviation Ltd from December, 3rd, 2016 to January, 31st, 2017.

The traverse lines were flown in the NS direction at azimuth of 0°-180° NE and were spaced at 100 m apart. The tie lines were flown in the orthogonal direction (east-west) and were spaced at 1000 m apart. The helicopter was flying at a mean speed of 80 km/h and at average altitude of 96 m above ground. The average ground clearance of the EM transmitter-receiver system was 50 m. The magnetometer average altitude above ground is 77 m (Figure 2).

The digital geophysical data were recorded on a PCMCIA flash card and then transferred to a field computer upon flight completion.

The VTEM and magnetic acquisition system was composed of the following equipment:

- VTEM™ Max in-loop system with peak dipole moment of 750, 000 NIA
- Geometrics high resolution magnetometer
- GPS navigation and positioning system
- Magnetic base station (Geometrics magnetometer)
- Radar altimeter

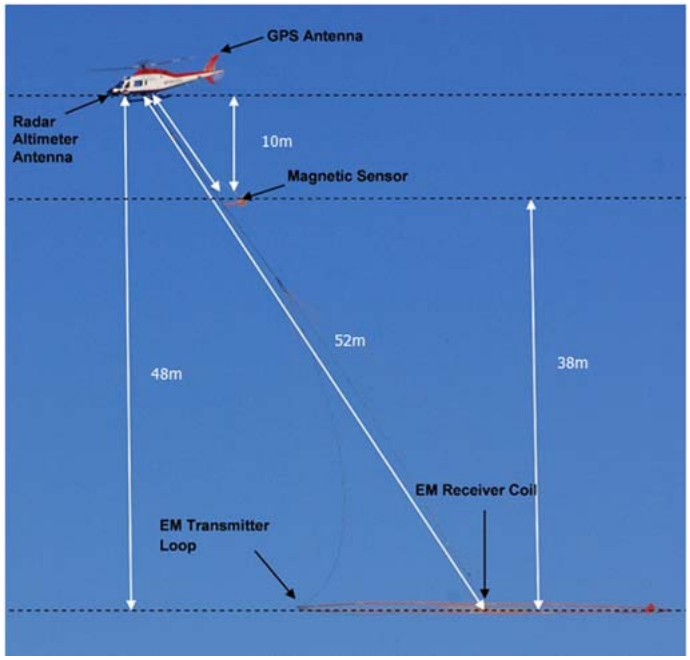

Figure 2: VTEM™ Max system configuration.

4. GENERAL CONSIDERATIONS

4.1 GEOLOGY AND MINERALIZATION OF THE SURVEY AREA

The property is primarily underlain by mafic volcanics intruded by a mineralized gabbroic intrusion. The area is covered by extensive glacial till with only local areas of out crop. Much of the regional geology interpretation is based on regional magnetic interpretation performed by the Ontario Geological Survey (OGS) and presented in Figure 3. It depicts Early Precambrian felsic intrusive (quartz monzonite and diorite), mafic and ultramafic rocks (dominantly gabbro with minor peridotite), which have intruded into felsic and intermediate meta-volcanics, all crosscut by multiple north-south trending faults and Precambrian diabase dykes. Except for a few isolated northwest-southeast trending outcrops, a thick blanket of glacial till covers the land and as a result, most of the geology is interpreted from limited diamond drill hole information and ground magnetic surveys. The map shows the mineralized gabbroic intrusion underlying the property and extending approximately 2.5 kilometres to the southeast.

Rock sampling has revealed that the intrusion varies in composition from diorite near the surface into quartz gabbro and gabbro. In areas along the footwall contact, occurrences of pyroxenite have been recorded. Both grainsize and plagioclase abundance varies greatly throughout the gabbro. The footwall rocks in the vicinity of the mineralization vary from diabase to andesite to basalts. Along the remainder of the gabbro contact the footwall is interpreted from geophysics to be mafic volcanics. Clasts of the footwall andesite are observed throughout the gabbro and range in size up to ~40m across (Vanderklift et al., 2005).

Copper-nickel mineralization is generally restricted to the gabbro within close proximity of the footwall contact, although several weakly-mineralized, disseminated/blebby zones are perched within the gabbro. Two closely-related zones of gabbro-hosted Cu-Ni mineralization estimated at 518,000 tons (@ 0.42% Cu, 0.41% Ni) and 574,000 tons (0.15% Cu, 0.65% Ni) are delineated. The mineralization of interest consists of thin sheets of blebby, semi-massive, and massive pyrrhotite, pentlandite, and chalcopyrite haloed by disseminated and blebby zones. These sheets range in thickness, but are generally between 0.3m and 1.5m. The sheets are elongate both along strike and down dip. Four substantial sheets, interpreted to be contiguous, were recognized. On average, they are ~80 × 50m. The largest is approximately 115 × 40 m.

4.2 HISTORIC WORK

Prior to 1989, ground magnetic and EM surveys were conducted by various contractors (Mespi Mines Ltd, Hollinger, and Texasgulf). Follow-up of delineated magnetic and EM geophysical anomalies with drill-testing revealed the presence of Cu-Ni mineralization related to mafic rocks.

In 1989 Falconbridge conducted an airborne magnetic and horizontal loop EM (HLEM) geophysical survey covering twenty-two contiguous claims in the Loveland Township. However, the geophysical survey did not indicate any drill targets and most of the delineated conductive zones are suggested to be related to surficial sources.

In 2004, ground magnetic and HLEM surveys were conducted by Quantec Geoscience on the northeast of Enid Creek. The magnetic survey identified a north-northwest trending magnetic high to the north of

a gabbroic intrusion. However, the HLEM survey didn't reveal any conductors associated with this gabbroic body and the magnetic anomaly remains untested to date.

Around fifty holes were drilled in the property by various companies and were assayed for Cu-Ni-PGE mineralization. All holes are located in the western portion of the property. Combined, the drill holes delineate a gabbroic body that is at least 300 meters wide (east-west) by 800 meters long (north-south) and thickens from the southwest (40 meters) to the northeast (220 meters). However, based on geophysical interpretation, the gabbro intrusion size in the east-west direction is estimated to be approximately 3 km.

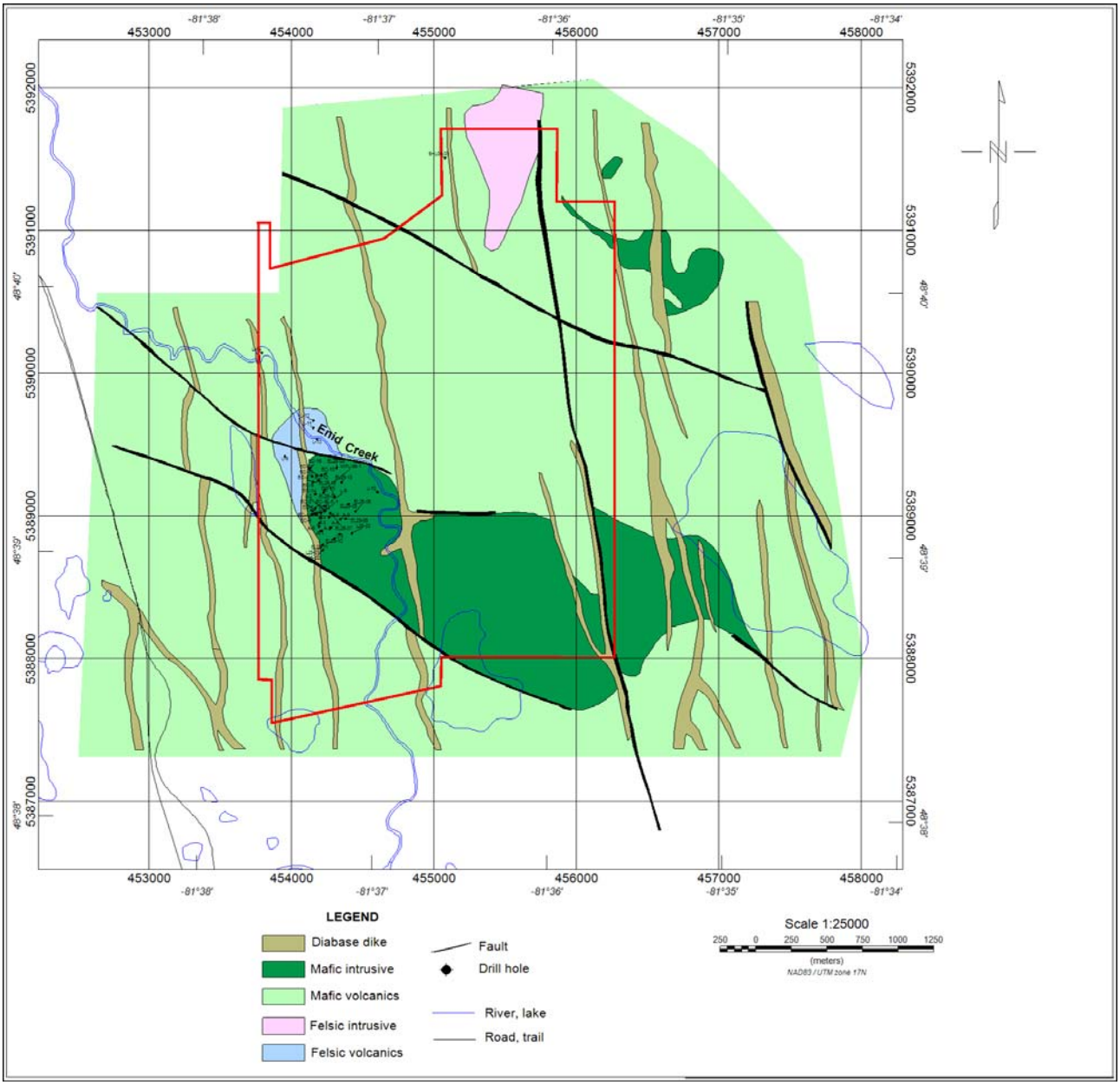

Figure 3: Geological map of the property (Ontario Geological Survey, after Gregory 2007, modified).

4.3 SURVEY DATA INTERPRETATION OBJECTIVES

The purpose of the helicopter-borne VTEM and the magnetic survey conducted on the survey area was to delineate new favourable target-areas for further detailed exploration of Cu-Ni-sulphide mineralization.

The data interpretation objectives were aimed to derive a detailed structural map of the property area, which highlights the structural control of mineralization emplacement and to delineate favourable target-areas associated with conductive zones for further exploration of mineralization. More specifically the data interpretation objectives are summarized in the following points:

- To derive a detailed structural map of the property;
- To delineate mafic and ultramafic rocks that may host or control copper-nickel-sulphide mineralization;
- To identify and map deep-seated conductive zones favourable for the exploration of nickel-sulphide mineralization.

To achieve these goals the interpretation efforts were based on magnetic and VTEM data transformations and their inversion results.

5. MAGNETIC DATA INTERPRETATION

5.1 OVERVIEW

Airborne magnetic surveys have long been used as a cost-effective technique for detailed geological mapping and mining exploration. They have been particularly useful for mapping remote and difficult-accessible areas thus offering a precious advantage versus ground surveys.

Advances in magnetic data processing and the availability of robust inversion software designed to invert the data in 1D, 2D and 3D dimensions have given the magnetic prospecting technique a new pulse as effective tool for litho-structural mapping in general and mining exploration in particular.

The use of standard and advanced filtering techniques via the Fast Fourier Transforms provides a good understanding of the structural framework of the study area, whilst the 3D inversion yields a tri-dimensional distribution of the rocks magnetic properties of the subsurface area with the main interest to help detect zones of interest including faults and structures controlling the mineralized zones, alteration zones and magnetite-bearing mineralized zones.

5.2 OBJECTIVES AND INTERPRETATION TOOLS

The magnetic data interpretation is initially based on the standard analysis of the acquired data and their transformations including reduced-to-the-pole, vertical and horizontal derivatives, tilt-angle derivative maps. It is also based on other more advanced approaches including edge and fault detection techniques, and 3D inversion inversions (Li and Oldenburg, 1996, Elis et al., 2012).

The main objectives expected from the magnetic data analysis and their inversion results are to derive a detailed structural analysis of the property, to generate a 3D distribution of the magnetic property of the subsurface area and to detect and delineate mafic and ultramafic intrusive bodies susceptible to host or control copper-nickel-sulphide mineralization.

One of the primary goals that are sought for during the structural interpretation of the magnetic data was to identify and delineate mafic structures (gabbroic intrusion) that may host copper-nickel-sulphide mineralization.

The main tools used for magnetic data analysis, interpretation and inversion are:

- Data transformation and filtering in the Fourier domain (Reduction to the pole, horizontal and vertical derivatives, analytic signal and other enhanced and filtered data using Geosoft Magmap algorithm in Oasis Montaj™);
- Fault Detection for structural analysis;
- 3D magnetic inversion using the Geosoft Voxi inversion software (Ellis et al., 2012)
- Structural and lithological analysis based on the transformed data and modeling results.

5.3 MAGNETIC INTERPRETATION PRODUCTS

The interpretation products obtained further to magnetic data analysis are provided in hard copy, digital format or both and include the following items:

- The present interpretation report (hard copy and PDF format);
- Structural map including minor and major faulting systems (PDF and Geosoft format);
- 3D magnetization and 3D magnetic susceptibility models (Geosoft database and voxel format);
- Magnetization and magnetic susceptibility depth slices (PDF and Geosoft grid format);
- Magnetization and magnetic susceptibility sections (PDF and Geosoft grid Format).

The magnetic data interpretation was based on the transformed maps by using the Fourier transforms and the 3D magnetic inversion outcomes. The aim of the magnetic data interpretation was to derive a detailed structural interpretation that includes faults, dikes and magnetic structures of mafic nature and to determine the magnetic properties (susceptibility magnetic and magnetization) of rocks and geological formations composing the subsurface area. Several transformed maps (horizontal and vertical derivatives, tilt-angle derivative and analytic signal) were used to assist the magnetic interpretation.

5.4 TRANSFORMED MAPS ANALYSIS

Magnetic data transformation was performed in the Fourier domain using the Geosoft MAPGAMP filtering module in Oasis Montaj™. Elements of structural interpretation results (presented and discussed in section 5.6) obtained from the 3D magnetic inversion and consisting of inferred faults, dikes and outlines of magnetic structures are superimposed on all transformed maps for illustration

purposes. First, a reduced to the pole (RTP) map is produced, since the RTP data are used for subsequent data filtering, transformation and analysis. The RTP image of the property shown in Figure 4 indicates the presence of three narrow and linear anomalous zones of magnetic high and stretching in the NS direction roughly. These linear anomalous zones correlate with inferred magnetic dikes of probably mafic nature (diabase). There are two zones of magnetic low observed in the northeastern part of the study area, correlating with inferred felsic rocks.

Figure 5 illustrates the 2nd vertical derivative calculated from the RTP data. It highlights the effect of near-surface features associated mainly with mafic volcanic dikes, mafic intrusions and fault structures that affect the study area. However, the inferred mafic dikes from the 3D MVI inversion are not located on the peaks of the 2nd vertical derivative image as they seem to be shifted by a certain distance. This offset can be explained by the occurrence of strong remanent magnetization in the mafic dikes. The presence of strong negative anomalies aligned along the positive anomalies, observed in the central and eastern parts of the grid are more likely indicating the presence of remanent magnetization in mafic rocks.

The tilt-angle derivative grid shown in Figure 6 provides a more focusing image of the NS trending narrows features associated with mafic volcanic dikes. The tilt-angle transform helps identify numerous faults striking mainly in the NE and NW direction. Similarly, a shift explained by the presence of remanent magnetization is noticeable between the peaks of the tilt-angle derivative image and the location of the mafic dikes inferred from the 3D MVI inversion.

The analytic signal (or total gradient) map shown in Figure 7, which is used to delineate magnetic structures such as mafic dikes and mafic intrusion does not seem to be strongly affected by the possible presence of remanent magnetization since there is no significant shift between the peaks of the analytic signal grid and the location of the inferred dikes from the 3D MVI inversion. Additionally, the analytic signal image gives a clear delineation of mafic rocks (probably associated with gabbroic intrusions) that are suggested to be present in the western and eastern parts, occurring along the NS dike structures.

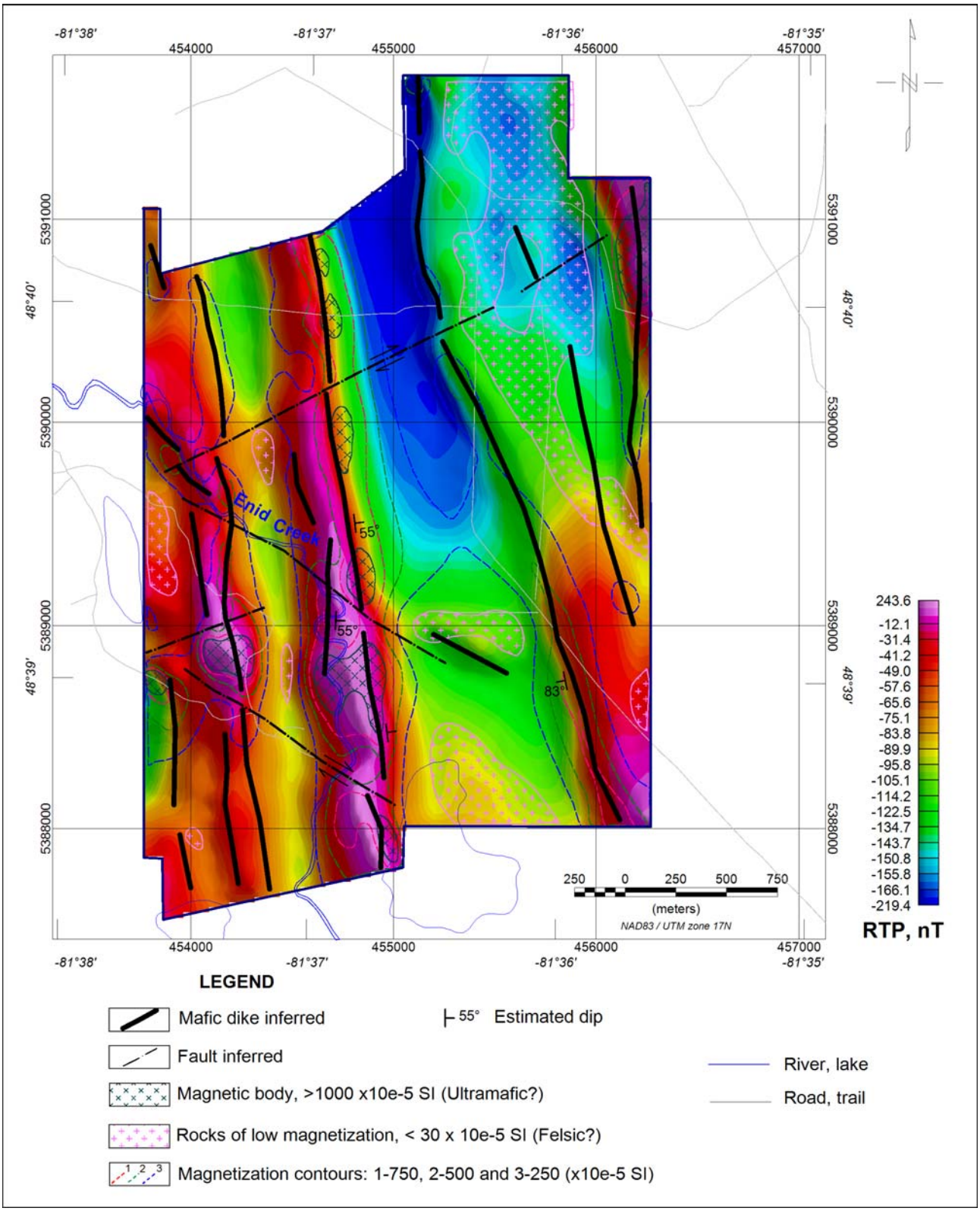

Figure 4: RTP image of the study area with superimposed inferred structural elements.

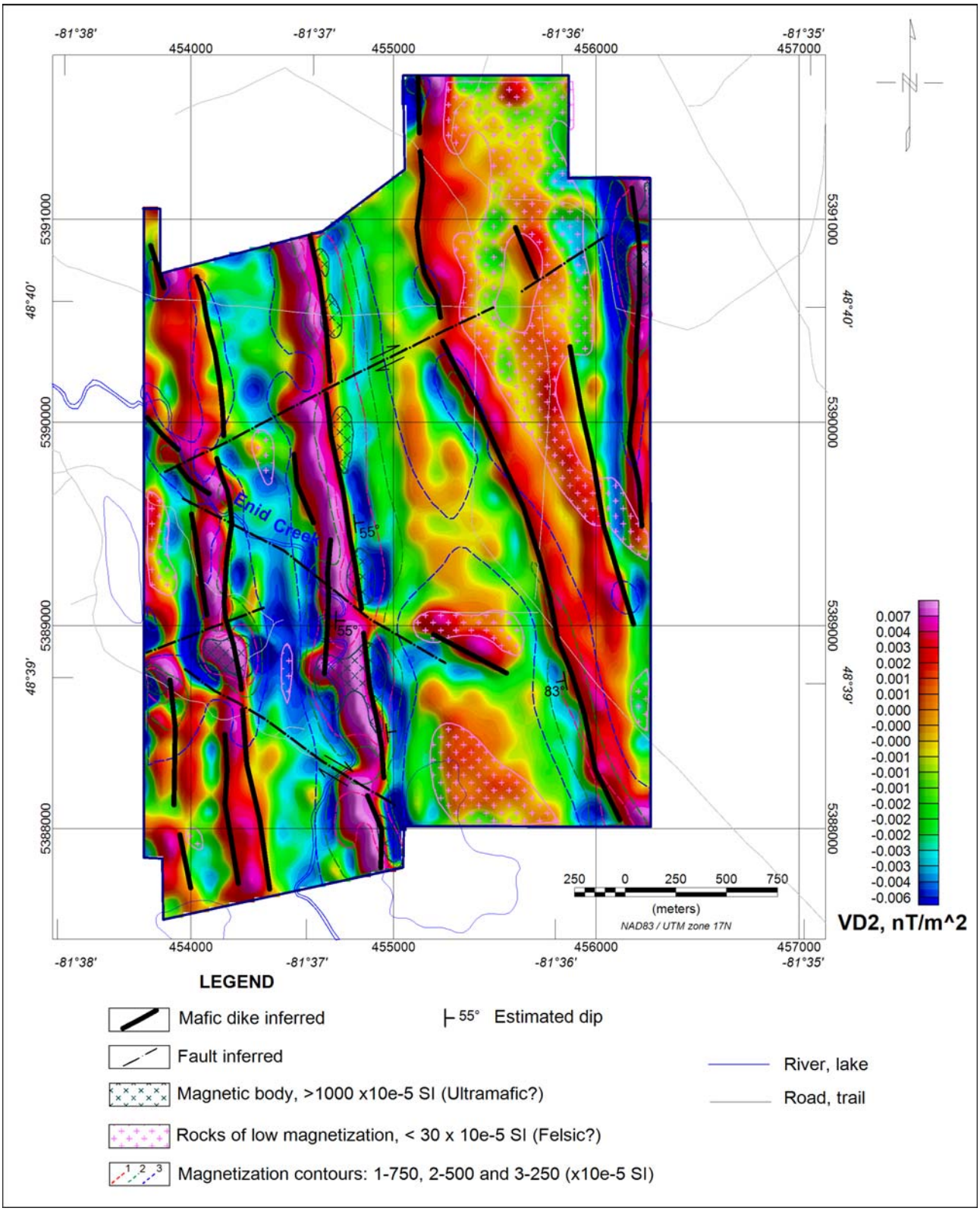

Figure 5: 2nd vertical derivative of the study area with superimposed inferred structural elements.

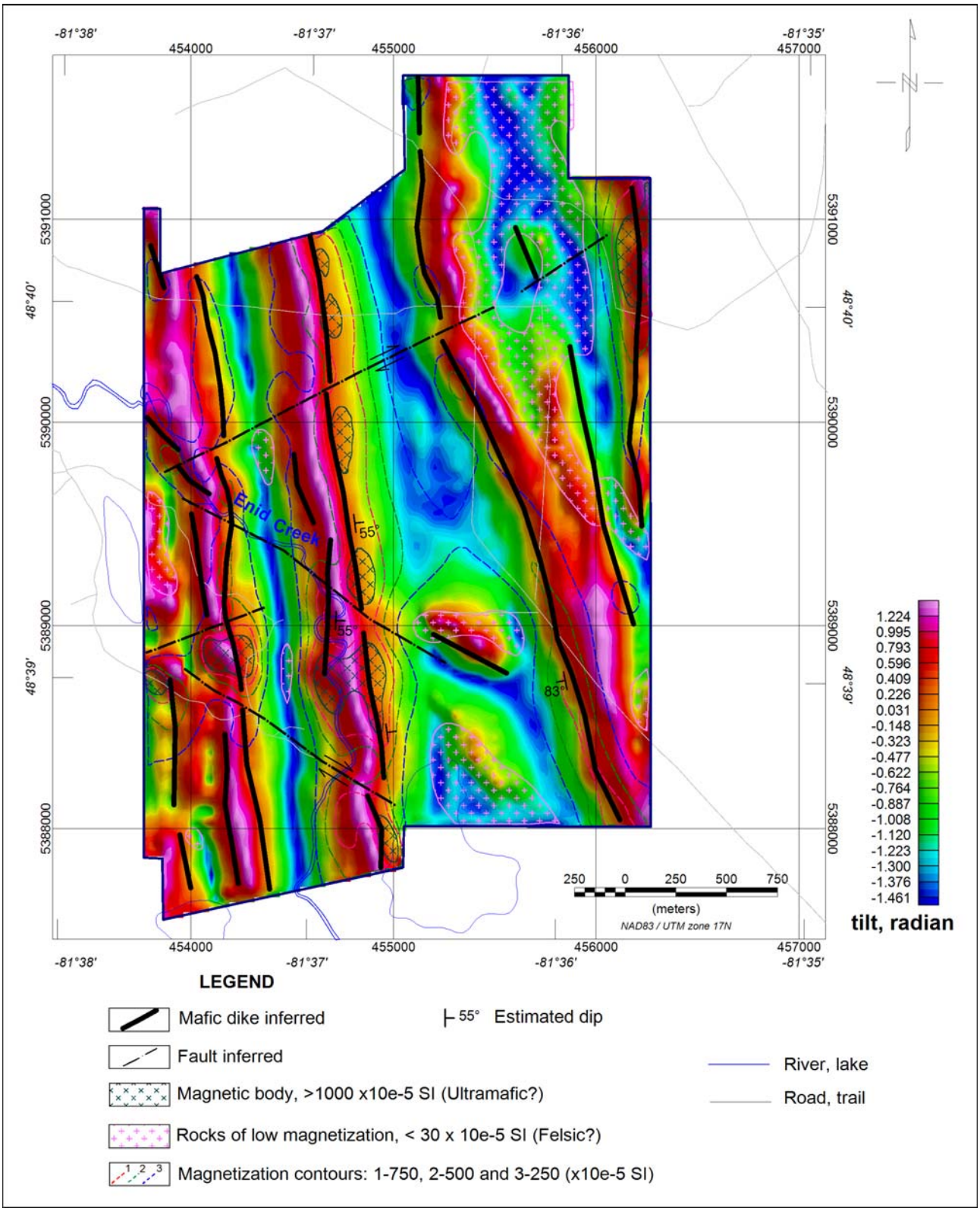

Figure 6: Tilt-angle derivative of the RTP image of the study area with superimposed inferred structural elements.

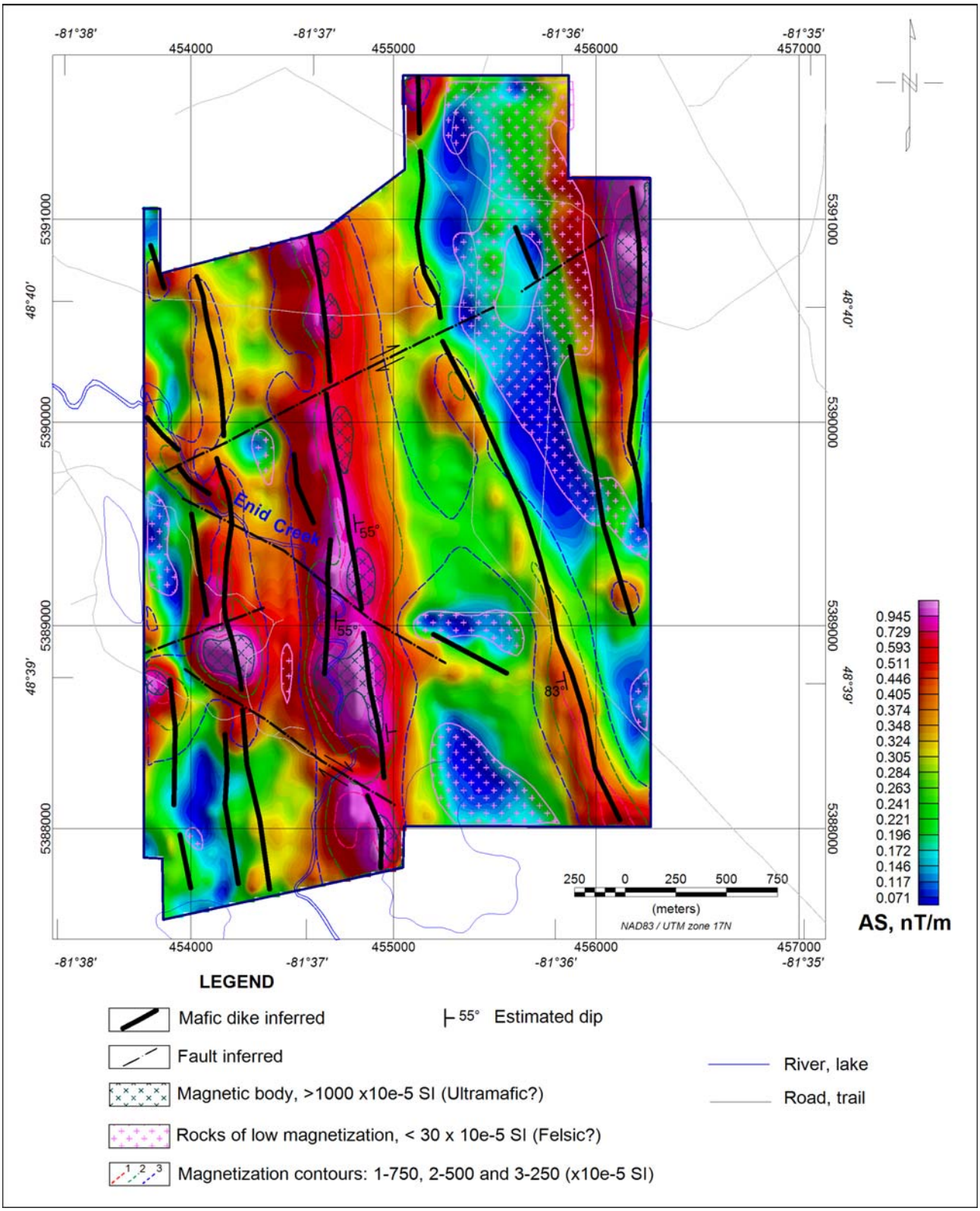

Figure 7: Analytic signal of the RTP image of the study area with superimposed inferred structural elements.

5.5 3D MAGNETIC INVERSION

The acquired magnetic data were inverted in 3D using the Geosoft VOXI software (Ellis et al., 2012) to recover both magnetic susceptibility and magnetization of rocks composing the subsurface area.
The Magnetization Vector Inversion (MVI) results revealed more reliable than those obtained with the magnetic susceptibility inversion results due to many advantages and primarily the account for the remanent magnetization occurring in mafic rocks. Moreover, the MVI inversion provides the tree components of the magnetization vector and its direction.

The residual (IGRF and trend-removed) total magnetic intensity data (TMI) were used to invert the observed data and to recover the 3D Magnetization Vector Amplitude model. The inversion was carried out with the inclusion of the topography by using the Digital Elevation Model (DEM) channel derived from the airborne geophysical survey.
A mesh size of 25 × 25 m in the horizontal direction, corresponding to ¼ line spacing was used to build the starting model. The size of the mesh in the vertical direction is variable starting from 10 m for the first 100 m, then gradually increasing by an expansion factor of 1.08 until depth of 1 km. The core model that encompasses the inversion area of interest was expanded laterally and vertically by 5 cell-paddings to avoid edge effects in the recovered 3D model solution. Both magnetic susceptibility and magnetization inversions were carried out with no constraints using a homogenous half space of 0 SI.

The recovered 3D magnetic susceptibility and 3D magnetization amplitude models are represented as 3D voxels in Figure 8. The magnetic susceptibility is expressed in SI units and the magnetization amplitude values are expressed in units normalized to SI units. The negative values observed in the magnetic susceptibility model (left hand side of Figure 8) do not have a geological explanation, and in fact, these are artefacts caused by the presence of remanent magnetization. By contrast, the 3D magnetization model (right hand side of Figure 8) provides a more realistic geological model, in which the features of elevated magnetization are attributed to mafic dikes.

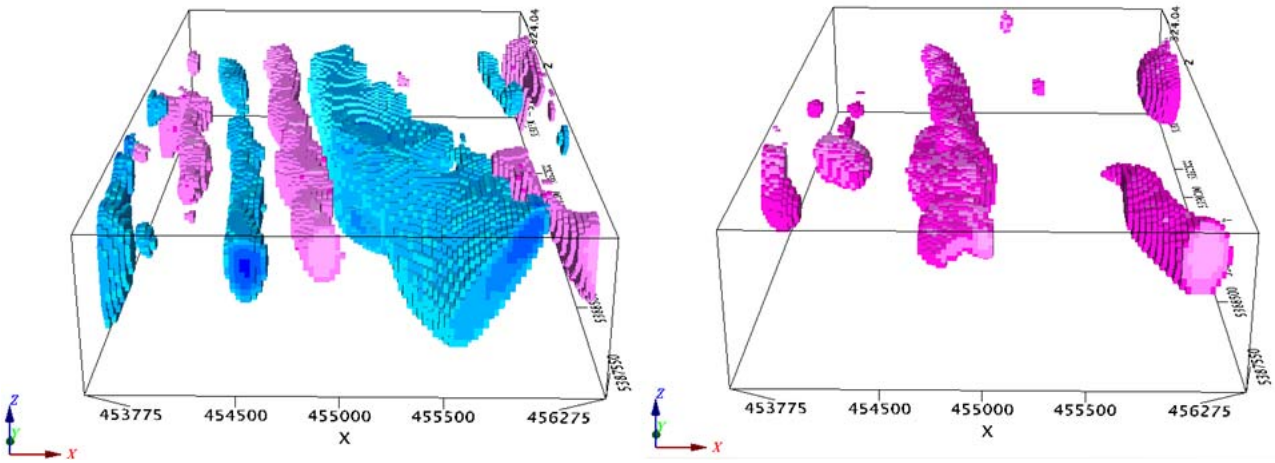

Figure 8: left, 3D magnetic susceptibility voxel model with clipped values (blue <-150×10^{-5} SI and pink >1000×10^{-5} SI) and right, 3D MVI voxel model with clipped values (pink >500×10^{-5} SI). View looking north.

Figure 9 highlights a magnetization isosurface (750×10^{-5} SI) with superimposed magnetization vectors, represented by arrows. The Figure clearly shows that the direction of the resulting magnetization is different to the inducing magnetic vector, whose inclination and declination parameters given by the

IGRF model are 73° and -10°, respectively. The resulting magnetization that shows an overall declination of 90° and near-horizontal inclination indicates more likely the presence of a remanent magnetization in the magnetic sources acquired during a period when the Earth's magnetic Field direction was different from the present day's Earth's magnetic Field.

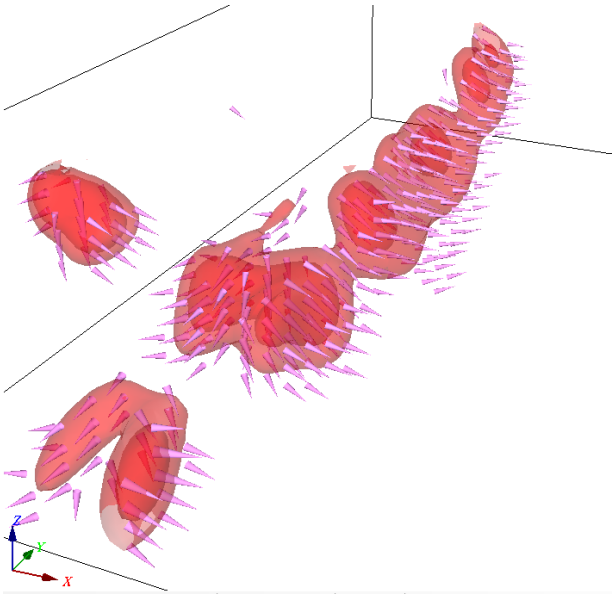

Figure 9: Magnetization isosurface (750×10^{-5} SI) with magnetization vectors represented by arrows.

The 3D inversion outcomes are presented as 3D Geosoft voxels (magnetic susceptibility model, magnetization amplitude model, magnetization vector direction and magnetization projection), depth slices ranging from the surface to depth of 800 m at 50m interval and vertical sections for all of the survey lines. All these products are accompanying the interpretation report (Appendices B and C) and are provided in both map and digital formats.

Figure 10 depicts the magnetic susceptibility depth slice corresponding to the depth level of -50 m below the surface. It is noticeable that the image is similar to the tilt-angle derivative image presented in Figure 6. The map includes the plots of magnetic dikes and fault structures inferred from the 3D MVI inversion. As shown on the map, the magnetic susceptibility image does not provide accurate location of the mafic dike system. Moreover, the blue zones corresponding to negative magnetic susceptibility values are more likely attributed to artefacts caused by the presence of remanent magnetization. By contrast, the magnetization amplitude depth slice corresponding to the same depth level and displayed in Figure 11 gives a more realistic geological interpretation with accurate location of mafic dikes.

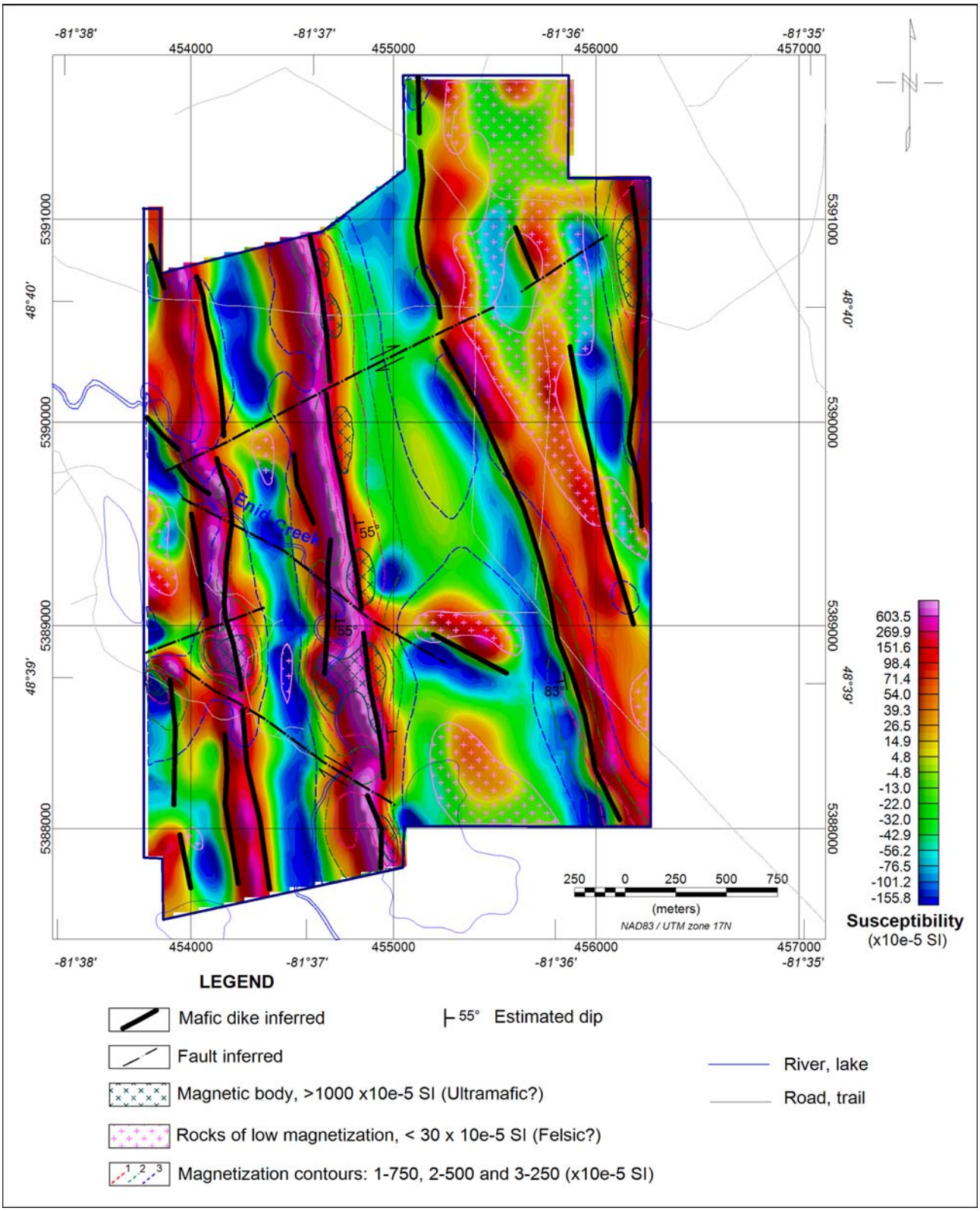

Figure 10: Magnetic susceptibility depth slice (-50m) of the property with superimposed inferred structural elements.

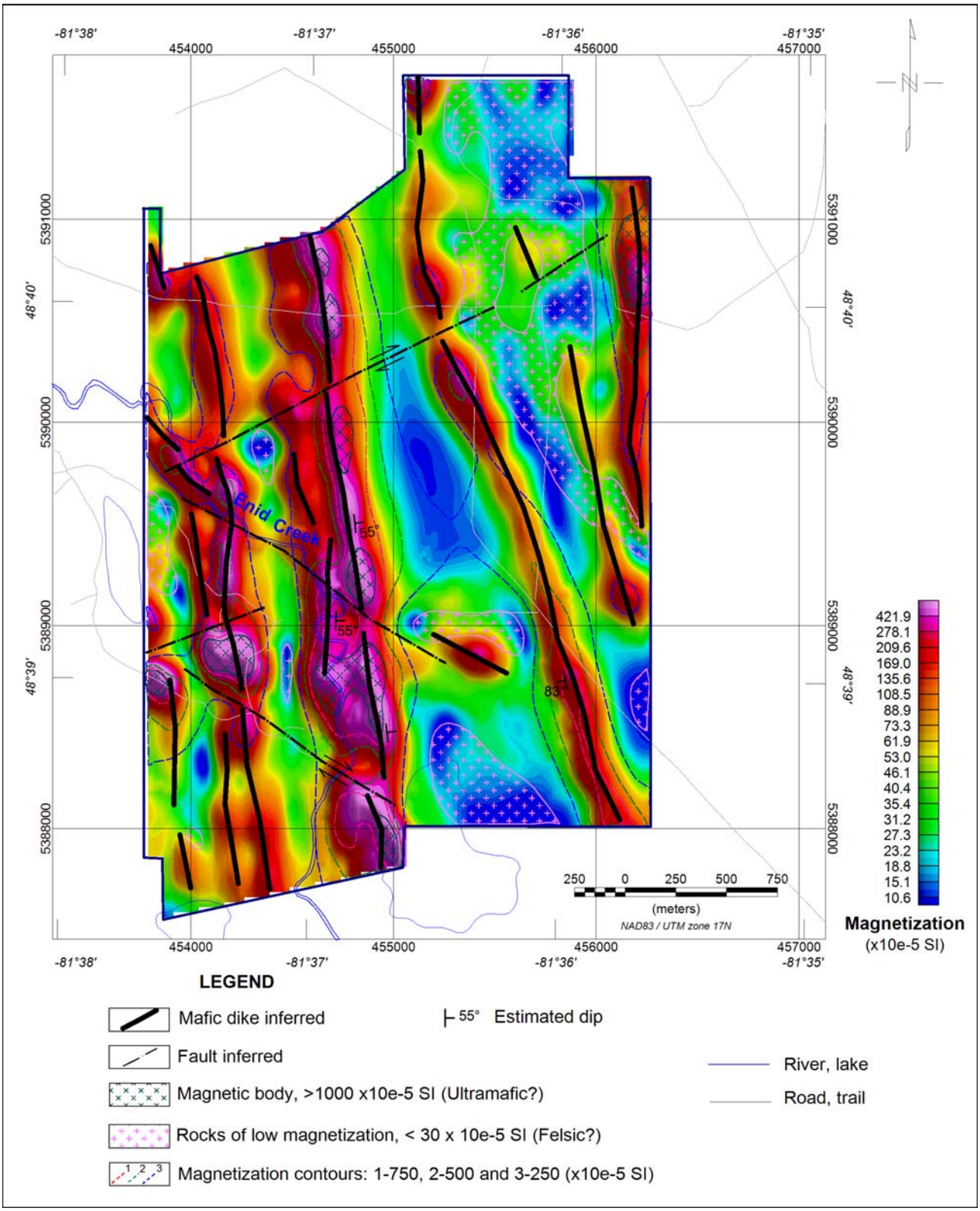

Figure 11: Magnetization amplitude depth slice (-50m) of the property with superimposed inferred structural elements.

5.6 STRUCTURAL INTERPRETATION

A structural interpretation map, based on the analysis of the magnetic data, their transforms and the 3D magnetic inversion outcomes has been derived and presented in Figure 12. The structural interpretation map includes inferred mafic dikes and faults, magnetic structures outlines and zones of low magnetization amplitude. It also includes contours of the 3D magnetization model projected on the horizontal plan. There are numerous dikes of more likely mafic volcanic nature (dolerite or diabase) striking in the NNW direction at azimuth of 10-20° NW existing within the survey area. In the western portion of the survey area, the dikes are suggested to dip easterly at shallow angles of around 55°, whereas in the eastern portion, they are either vertical or steeply dipping south-westerly.

The entire dike system appears to be affected by dextral faults striking in two preferred directions (northeast at azimuth of 60° NE and northwest at azimuth of 55° NW). Moreover, the interpretation suggests the presence of several magnetic bodies of elevated magnetization (> 1000×10^{-5} SI units) of probably mafic to ultramafic nature occurring along the dike system and more particularly in the western portion of the survey area. These magnetic bodies that appear as somewhat stretched in the NS direction may be linked to gabbroic intrusions. Mapping these gabbroic intrusions is important for base metal mineralization exploration since they can host copper-nickel mineralization.

The eastern portion of the property is dominated by the occurrence of large bodies of low magnetization (<30×10^{-5} SI units) interpreted as being linked to felsic volcanic and felsic intrusive rocks.

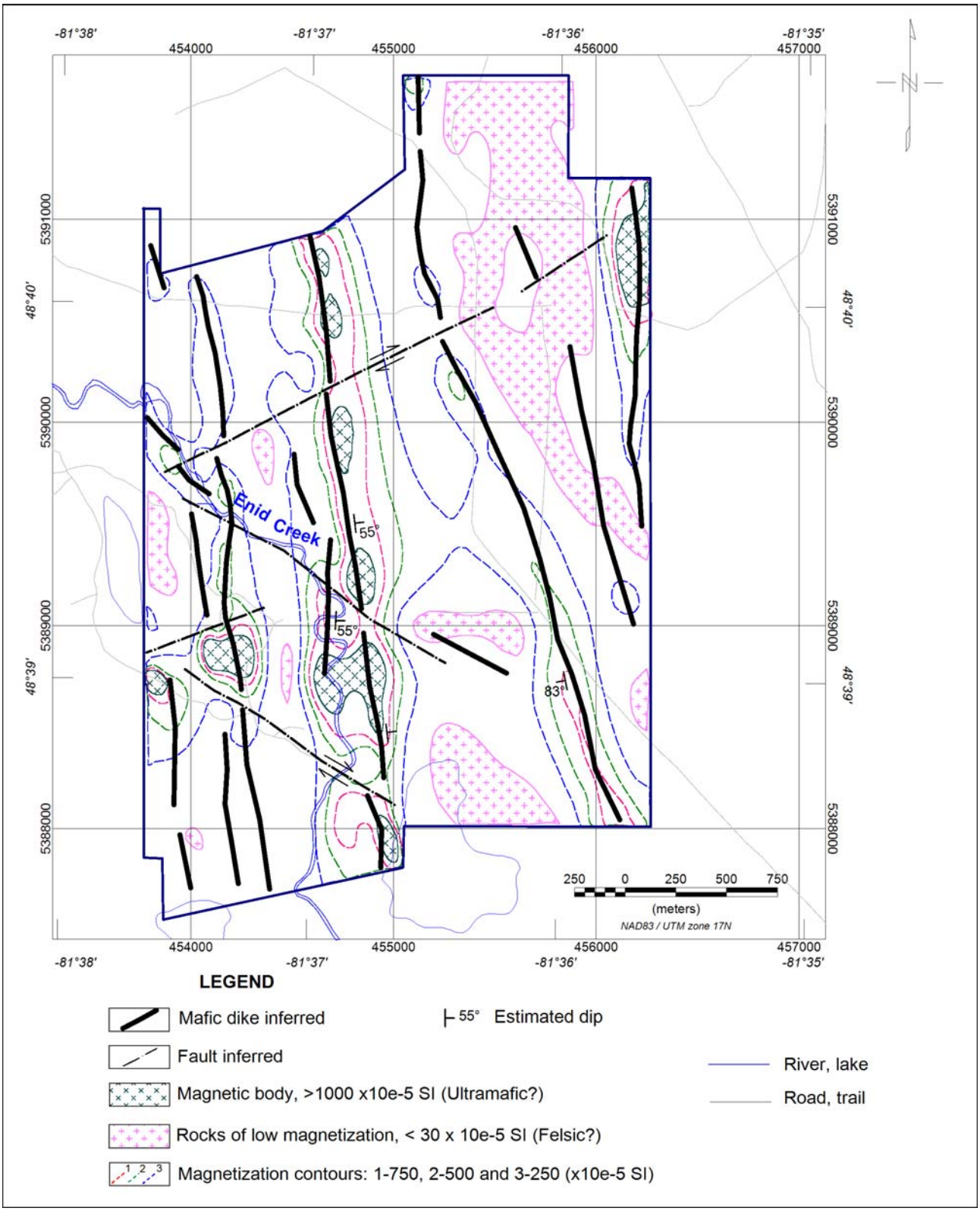

Figure 12: Structural interpretation map of the property inferred from the magnetic data.

6. VTEM DATA INTERPRETATION

6.1 OVERVIEW

The VTEM helicopter versatile time-domain electromagnetic (TDEM) system was introduced into commercial use in late 2002 (Witherly et al., 2004). Since then, Geotech Ltd has been continuously improving the system in terms of signal to noise reduction and operational reliability.
The VTEM™ max system uses the concentric loop (in-loop) geometry, with a large transmitter loop of 35 m in diameter and a smaller receiver of 1.1 m in diameter situated in the centre of the transmitter. The transmitter waveform is generated with 30 Hz base frequency and the peak dipole moment is around 750,000 NIA. The VTEM system is one of the most popular TDEM systems in commercial service. It features the highest signal to noise ratio in the industry, providing superior depth of investigation. The in-loop transmitter-receiver configuration provides symmetric responses to allow for intuitive conductor interpretation and high spatial resolution independently of flight line direction. Low base operating frequency allows EM signal penetration through conductive overburden.

Since 2011, VTEM system has been upgraded to the full waveform (VTEMplus). The significant features of the VTEM full waveform system are (Legault et al., 2012):

- Streamed half-cycle recording (192 kHz) of transmitter and receiver waveform data;
- Continuous system calibration corrections;
- Transmitter-drift and parasitic-noise corrections (Macnae and Baron-Hay, 2010);
- Ideal waveform deconvolutions (Annan, 1986).

These features lead to improvements in reliable EM data in the 0.018-9.256 millisecond decay time range, providing more accurate (<50 m) minimum depth resolution for groundwater and near-surface applications while maintain great depth-penetration capability of up to 400 m for deap-seated mineralization exploration (Prikhodko et al., 2010).

5.2 OBJECTIVES AND INTERPRETATION TOOLS

The objectives of the VTEM survey carried out over the survey area are outlined in the following points:

- To detect and map conductive zones related to nickel-sulphide mineralized zones;
- To estimate depth and shape of delineated conductive targets;
- To provide a resistivity (or conductivity) distribution of the near surface area.

To achieve the outlined objectives the following standard and advanced interpretation tools were used during the data analysis/interpretation process:

- Decay and Time Constant (Tau) analysis and interpretation using in-house built software;
- EM anomaly centres detection and anomaly categorization using in-house built software;
- 1D inversion using Layered Earth Inversion software;
- Interpretation and targeting analysis using advanced prediction techniques;
- Prioritization of the VTEM anomalies for Ni-sulphide mineralization targeting.

6.2 EARLY TIME DECAY ANALYSIS

Airborne EM techniques have long been used as a very effective tool for the exploration of nickel-sulphide mineralization. Usually, nickel and copper ore bodies exhibit high electrical conductivity that can easily be detected by airborne EM systems. The primary use of the VTEM technique is therefore, to map conductive zones associated with nickel-sulphide mineralization zones. In general, the early time EM response can be used to characterize the electrical properties of the near-surface geology such as overburden. At the early time stage, the eddy currents are gathering in the near surface area and therefore, the secondary fields measured at the receiver reflect the electrical properties of the shallowest part of the earth. At the mid- and late time stages, the eddy currents are gathering deeper and consequently, the secondary fields measured at the receiver will reflect the electrical properties of the deeper part of the earth limited by the depth of investigation. Consequently, the mid and late time data are more useful for detecting deep-seated conductive mineralized ore bodies.

Figure 13 displays the mid-time channel 25 corresponding to the measured decay at 0.44 ms after the current shutoff. The map indicates the presence of a series of interesting anomalies in the western part of the survey area and occurring along the Enid Creek. The two westernmost anomalies have been drill-tested and the diamond drilling results confirmed their link to mineralized zones. However, the southern anomalies remain untested to date. Moreover, the map shows the evidence of weaker anomalous zone occurring in the central area and stretching in the NW direction over a distance of 2 km approximately. It may represent a deep-seated moderate conductor. Figure 14 displays the late-time channel 40 corresponding to the measured decay at 5.31 ms after the current shut off. Only the anomalies observed in the western portion are remaining at this late time and there is no noticeable response elsewhere in the survey area.

6.3 TIME CONSTANT (TAU) ANALYSIS

The time constant (tau) is calculated from decay analysis via in-house built software. The algorithm uses a sliding window from early time to late time to estimate the time constant (tau) using a linear regression. Time constant is an important parameter and is related to source electrical conductance. Tau also serves as a guide for determining the conductor quality; poor conductors exhibit short (or low) taus, whereas good conductors usually exhibit long (or high) taus.

Figure 15 depicts the Tau image calculated from the dB/dt-z channels. It indicates the presence of several anomalous zones with the strongest ones occurring along the Enid Creek in the western portion of the survey area. There is one interesting but weaker anomaly occurring in the central area and one anomaly, in the northeastern portion of the survey area. The time constant image calculated from the B-z data and shown in Figure 16 gives a better definition of the western anomalies and it better highlights the central weakly conductor.

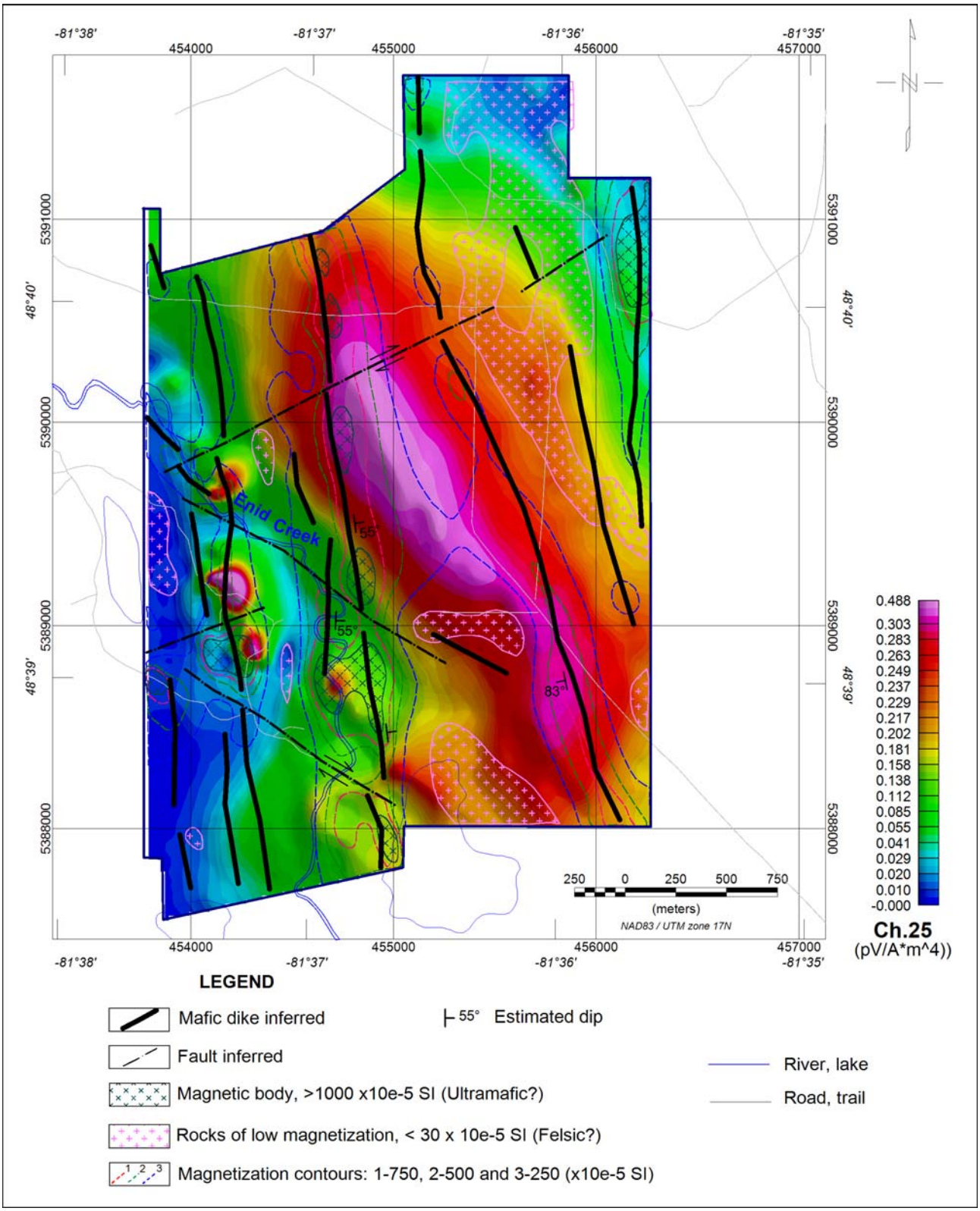

Figure 13: dB/dt-z mid-time channel (0.44 ms) grid image including magnetic interpretation results.

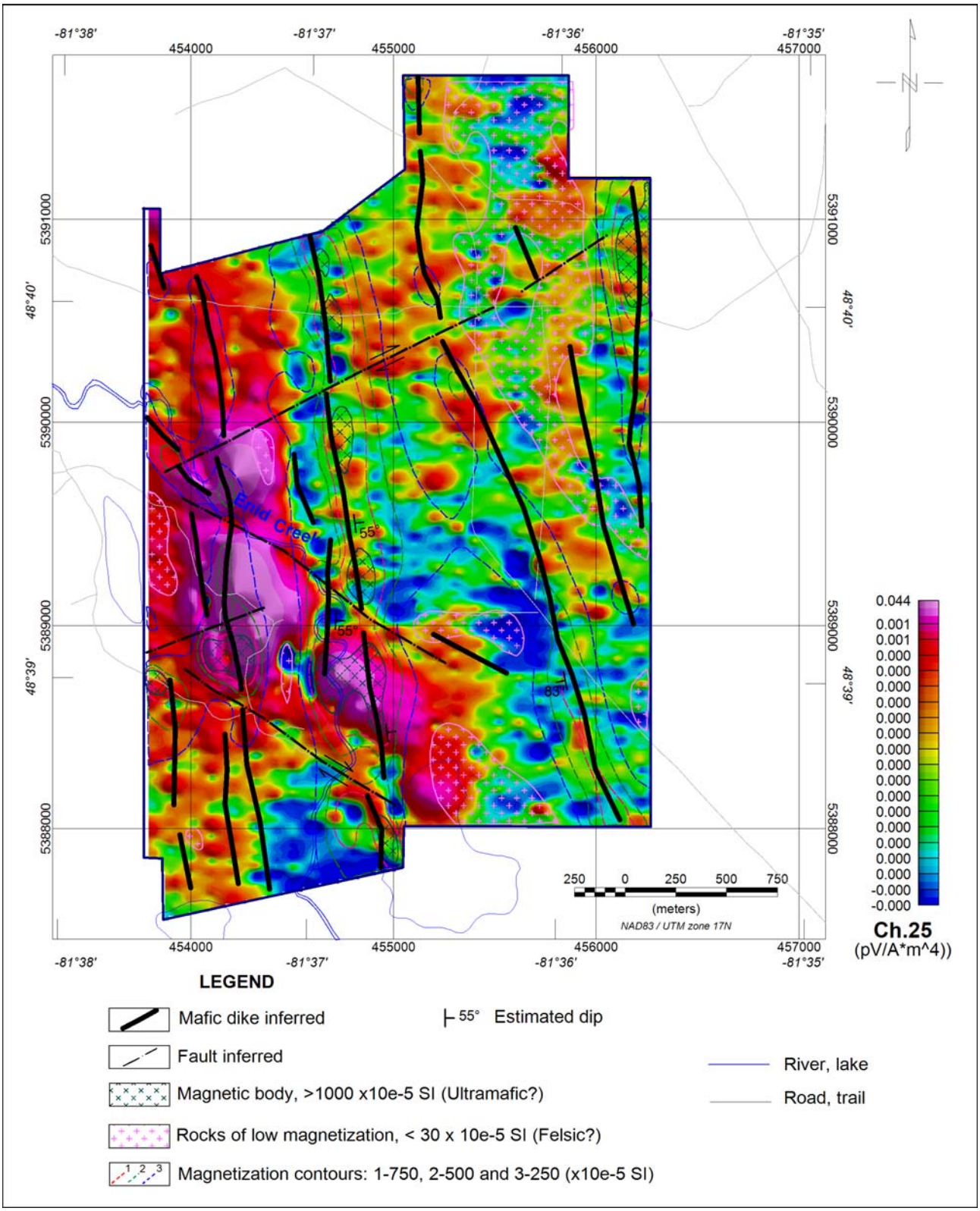

Figure 14: dB/dt-z late time channel (5.31 ms) including magnetic interpretation results.

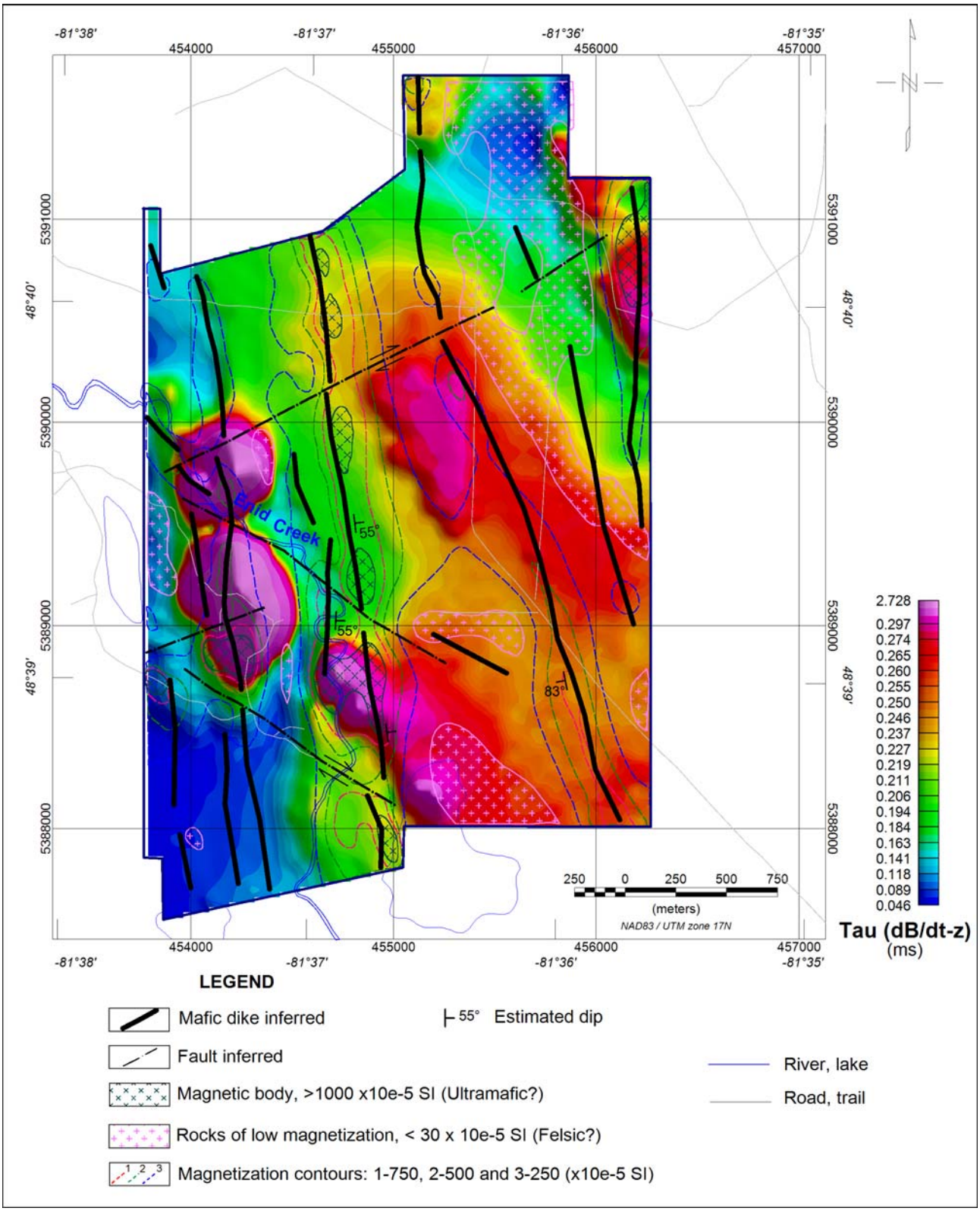

Figure 15: dB/dt-z time constant including magnetic interpretation results.

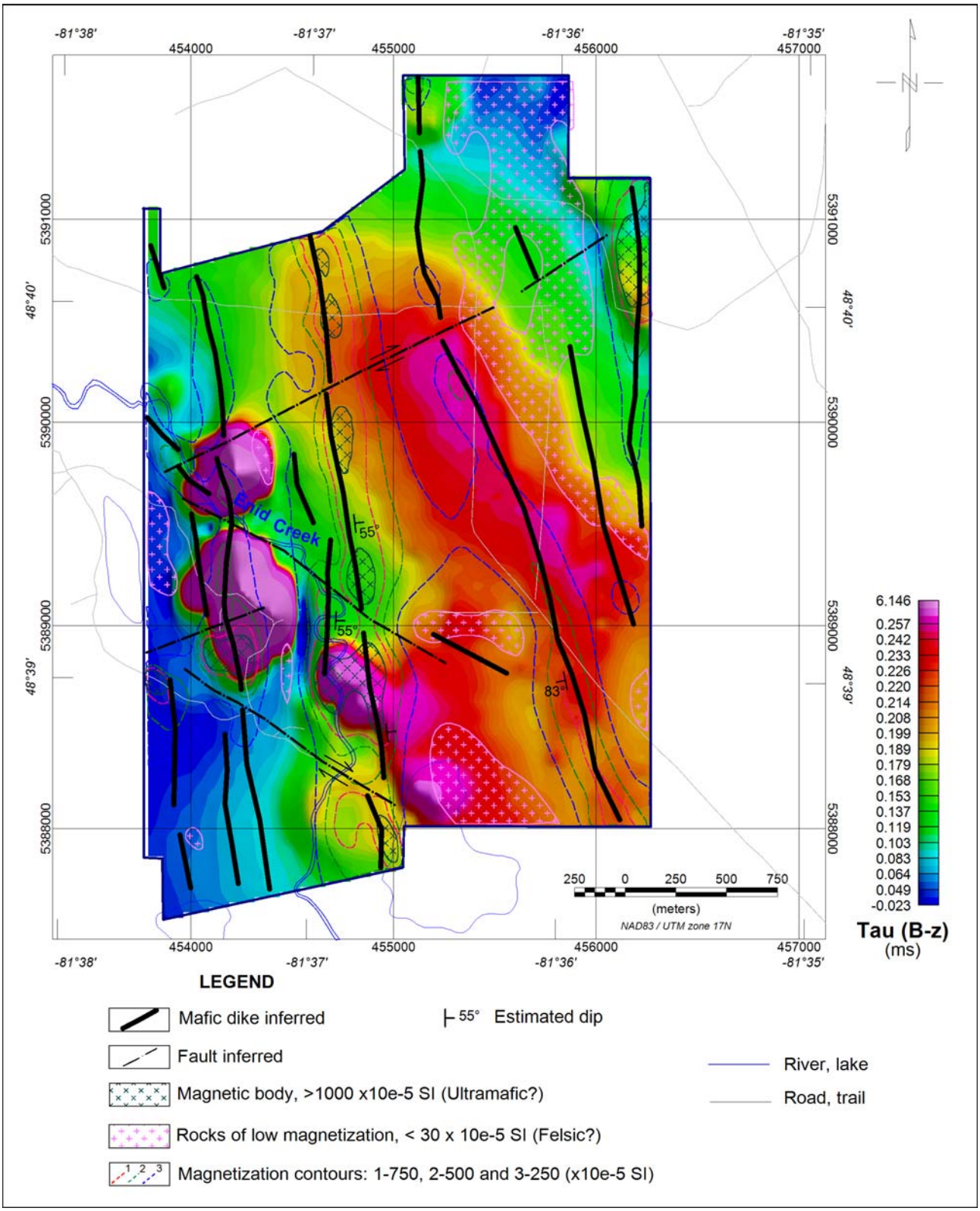

Figure 16: B-z time constant including magnetic interpretation results.

6.4 1D INVERSION RESULTS

6.4.1 OVERVIEW

The VTEM data interpretation was based on the VTEM decays, time constant analysis, and the resistivity inversions. Resistivity depth transform or resistivity depth imaging (RDI) was carried out using Geotech proprietary software, which is based on algorithm described by Meju (Meju, 1998).
Additionally, we performed a 1D inversion of the entire VTEM survey data using the 1D GALEI (Brodie, 2015 and 2016). GALEI is a 1D AEM forward modelling and inversion program developed by Geoscience Australia (Brodie, 2015 and 2016) and released to the public on GitHub:

(https://github.com/GeoscienceAustralia/ga-aem.git).

For the 1D inversion, we used the smoothed inversion style, in which the Earth is discretized into 33 layers with fixed thicknesses increasing with depth from 3 to 50 m and we solved for conductivities.
The 1D inversion was performed with a starting LE model composed of a homogenous conductivity model equal to 0.001 S/m and with no constraints applied to the starting model layers conductivities.

Initially, the 1D inversion results were obtained for all flight lines as 1D conductivity model sections, and then the results were stitched and gridded in 3D to obtain a 3D voxel conductivity model of the subsurface area limited on top by the topographical relief and on bottom, by depth of 400 m (corresponding approximately to the system depth of investigation), (Figure 17). RDI and 1D model sections for all survey lines are provided with this report. Additionally, a series of apparent resistivity (from RDI) and electrical conductivity (from 1D inversion) depth slices ranging from 0 to 400 m at 25 m interval were extracted and included with the deliverables.

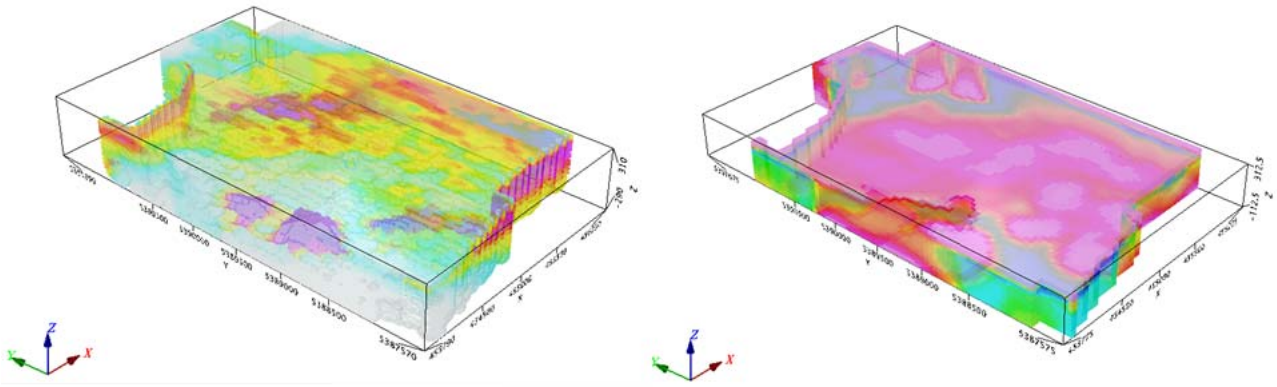

Figure 17: Left, RDI voxel and right, 1D conductivity voxel in transparency.

6.4.2 RESISTIVITY/CONDUCTIVITY DEPTH SLICES

A series of resistivity depth slices (from RDI) and conductivity depth slices (from 1D inversion) corresponding to depth range of 25 to 400m at 25m interval were extracted from the 3D voxel model and analysed. All these depth slices are presented in Appendices G and H of this report.

The purpose of the depth slices analysis is to study the resistivity changes from the surface to a depth of up to 400 m with the main interest of indenting and mapping conductive zones that may represent a particular interest for the exploration of nickel-sulphide mineralization.

Figure 18 illustrates the 1D conductivity depth slice for the depth of 150 m below the surface. It displays many local anomalous zones of elevated conductivity occurring mainly in the west and south of the survey area. The most significant one, located south of Enid Creek is associated with known copper-nickel-sulphide mineralized zone. There is a broad anomalous zone of moderately low conductivity occurring in the central area, stretching roughly in the northwest direction. The latter may indicate a link to a deep-seated conductor.

The apparent resistivity depth slice corresponding to the same depth level of 150 m below the surface and displayed in Figure 19 highlights mainly the same features as the 1D conductivity depth slice. However, the local zones of resistivity low mapped in the west and the south of the survey area appear of smaller size comparing to the 1D inversion results. Moreover, the resistivity depth slice provides a better definition of the broad anomalous zone located in the centre and stretching in the NW direction.

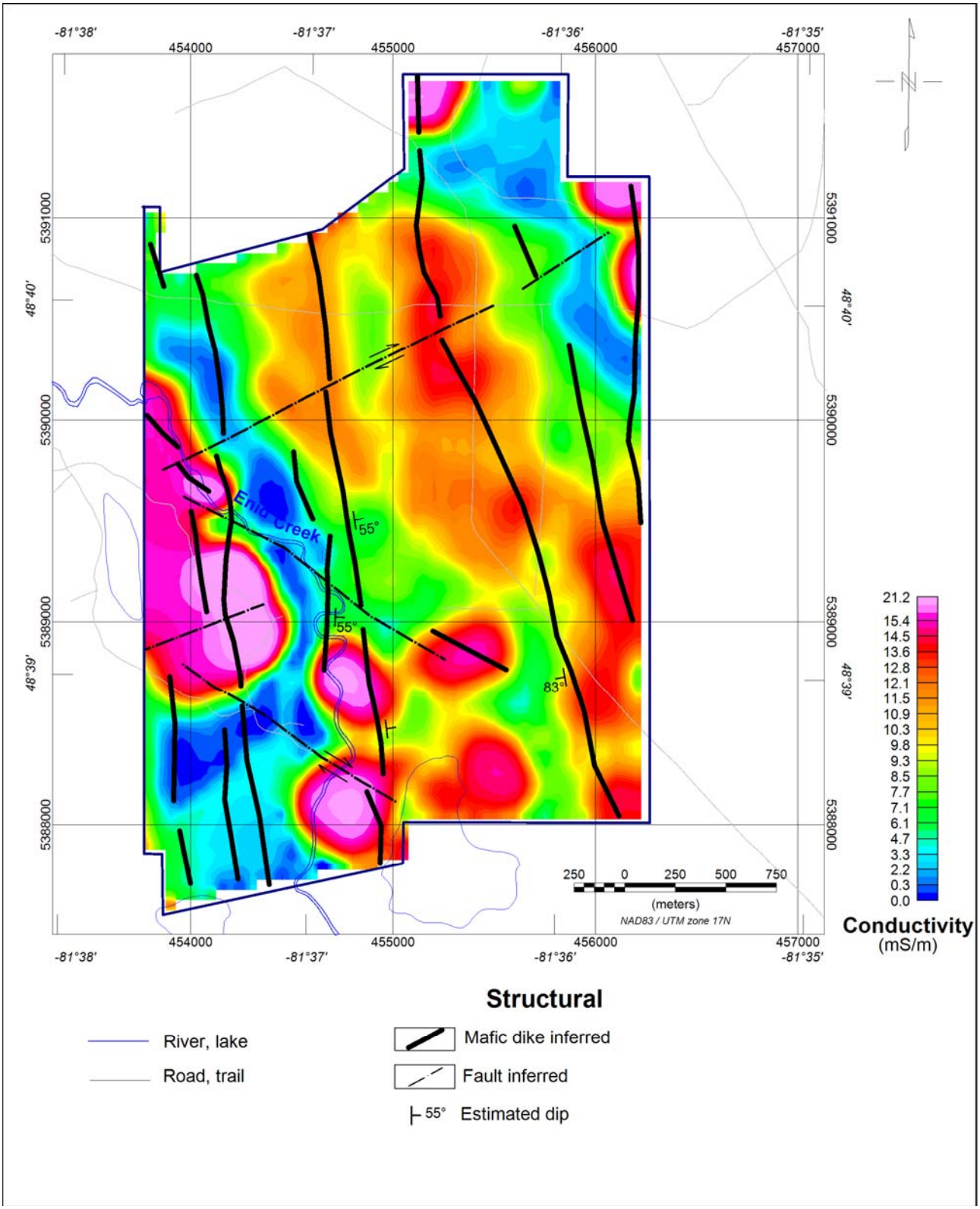

Figure 18: Conductivity depth slice for depth of 150m including magnetic interpretation results.

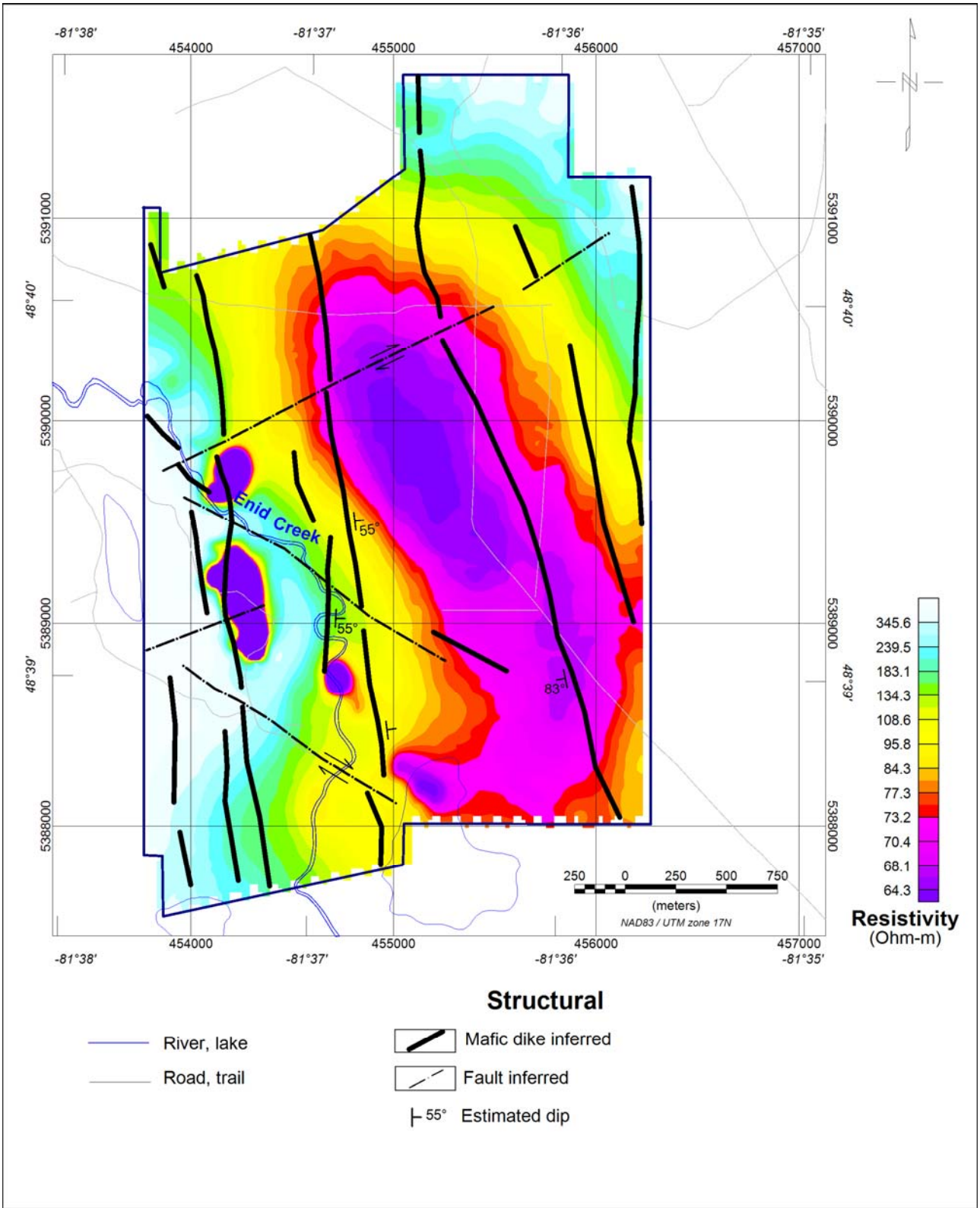

Figure 19: Resistivity depth slice for depth of 150m including magnetic interpretation results.

6.5 2.5 D INVERSION (PLATE MODELING)

A 2.5D EM inversion using the EMIT Maxwell plate modelling algorithm (Duncan, 1989) was performed on selected targets. The algorithm approximates conductive sources by either a thin or a thick plate. The 2.5 D modelling results for selected targets from the present survey area and other blocks are presented in a separate document.

The modelling results for the anomalies observed in the western portion of the survey area are suggesting the presence of shallowly dipping plates with estimated depths of 110m for plate A2 and 180 m for plate A3 (Figure 19). The estimated conductance values are 100 S and 80 S for plate A2 and plate A3, respectively.

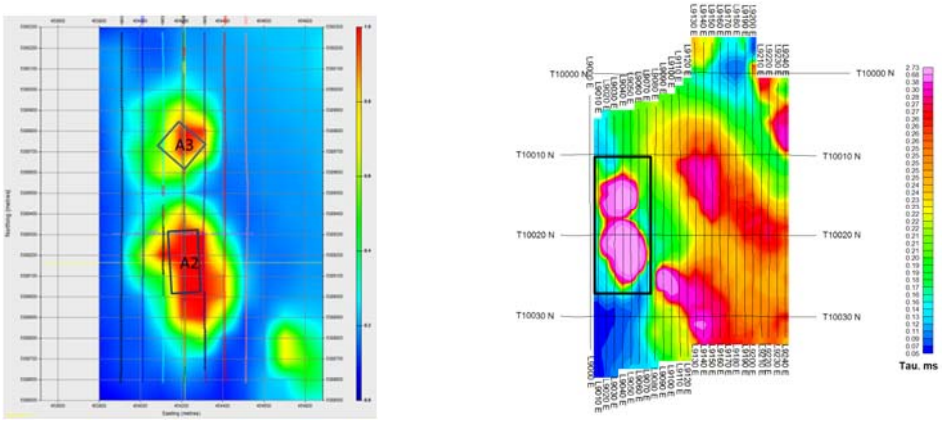

Figure 20: Left, modeled plates projected in the horizontal plan, and right, outline of the target area over the tau grid image.

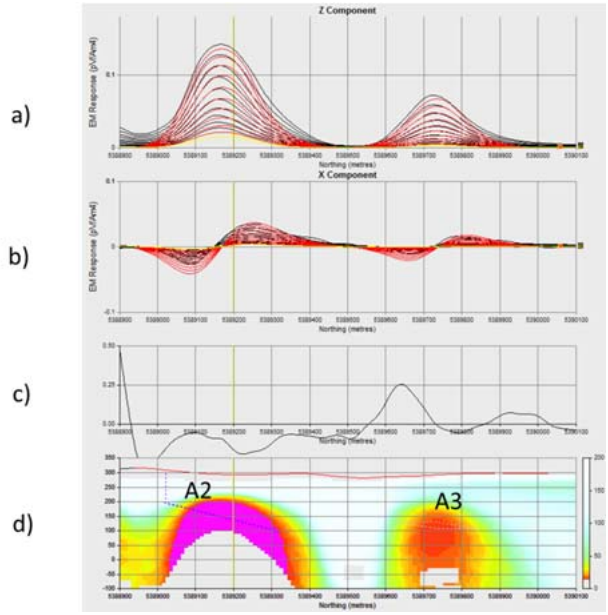

Figure 21: Modeling results; a) Observed (black) and calculated (red) dB/dt-z late time decays ; b) Observed (black) and calculated (red) dB/dt-x late time decays, c) Vertical gradient of RTP, and d) RDI section with Plates projection.

6.6 3D INVERSION

A Fast 3D inversion was performed on selected targets using the Fullagar's (Schaa and Fullagar, 2012) VPem3D algorithm on selected targets. VPem3D is not a full 3D inversion algorithm but a fast approximate 3D modelling and inversion program suitable for rapid 3D inversion of small target areas as well as of large data sets. It is also used for integrated interpretation of TEM data in concert with geological and other data.

VPem3D converts dB/dt or B-field TEM decays into Resistive Limits (RL) being the integral of the B-field decay over time or the integral of t·dB/dt over time. By transforming decays to RL, the multi-channel TEM inversion problem is effectively reduced to a single channel magnetic inversion, yielding a fast 3D inversion. For the unconstrained inversion the recovered model is expressed in time constant values (ms) rather than in resistivity or conductivity values.

In the present study we performed a 3D uncontained inversion on selected targets using the compact body inversion style to resolve the conductive sources. The results are presented as 3D voxel model and 3D DXF format.
The inverted target area (section 6.3) includes two anomalous zones. The inversion results shown in Figure 22 suggest that the south zone is located at shallow depth of 50 m approximately whilst the north zone is located at deeper level of 100 m approximately. For comparison purposes with the 2.5D Maxwell plate modelling results the plates are projected in the cross-section as shown in Figure 22. Depth estimates from the Vpem3D inversion results for the south target are in good agreement with the Maxwell plate modelling results (Plate A2), whereas they appear to be underestimated for the north target (Plate A3).

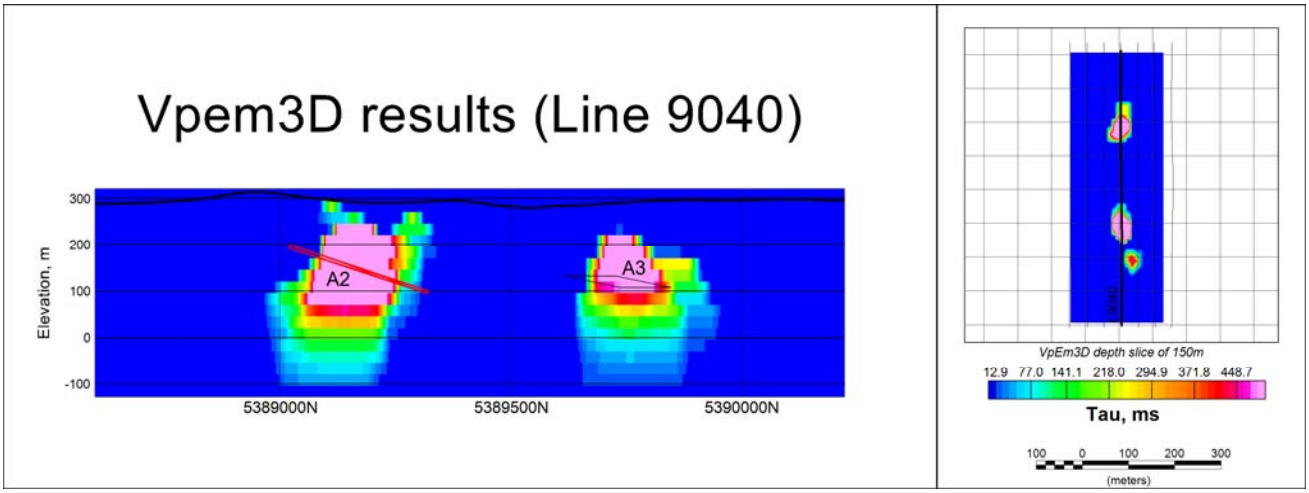

Figure 22: Vpem3D inversion results of the target area of section 6.3. Left, cross-sectional view of the 3D Modeling results with superimposed Maxwell plates projection and right, tau depth slice (depth of 150m with the section trace).

6.7 EM ANOMALY CENTRES

Figures 23 below depict the classified EM anomalies superimposed on the dB/dt-z time constant grid image. The Anomaly picking was performed on the profile data using a manual procedure. The EM anomalies are classified into six (06) classes and are represented by different symbols according to their conductance values, calculated from the time constant using a plate model. The conductance range varies from less than 5 Siemens to over 50 Siemens.
From the anomaly picking results six anomalous zones designated by label "An" and five conductor axes (linear conductors) designated by the label "C" were identified and delineated within the survey area that are described below.

A- Anomalous zones

An1- This anomalous zone is located in the western part of the survey area and west of the Enid Creek. It is by far the strongest and the most important anomalous zone by strength and size. It has an oval shape, stretching in the north-south direction roughly. Its size is 500 × 800 m approximately and it includes the strongest anomalies (>50 Siemens). Known nickel-sulphide mineralization is associated with this anomalous zone.

An2- This anomalous zone is located in the western part of the survey area and north of An1. Enid Creek runs between the two anomalous zones. This is the second most important anomalous zone by strength and size. It has a circular shape with a diameter of 500 m approximately. It includes several moderately strong anomalies ranging from 10 to 50 S.

An3- This anomalous zone is located in the southern portion of the survey area and it include anomalies of moderately low conductance values ranging from 5 to 10 S. The anomalous zone is stretching in the NW direction and has a size of 300 × 700 m approximately. It appears that this anomaly has not been tested to date.

An4- It is located in the southernmost portion of the survey area, south of An3. It includes anomalies of moderately low conductance values of less than 10 S. It is stretching in the NE direction roughly and has a size of 300 × 600 m approximately.

An5- It is located in the north-eastern corner of the survey area and is stretching in the NW direction over a distance of 500 m approximately. The estimated conductance is moderately low and not exceeding 10 S.

An6- This anomalous zone is located in the northeast of the survey area south of An4. It appears to be stretching in the NNW direction over a distance of 700 m roughly and includes moderately low anomalies (<10 S).

B- Conductors Axes

C1- This moderately poor conductor is located in the central area of the property and is characterized by an estimated conductance of less than 10 S. It is stretching over a distance of 1.6 km in the northwest direction. It appears to be linked to a deep-seated conductor.

C2- This linear conductor is located in the southernmost portion of the survey area and is stretching in

the NE direction over a distance of 700 m approximately. It exhibits a low conductance of less than 5 S.

C3- This conductor is located in the southwest and is stretching over a distance of 400 m. It exhibits a conductance value of less than 5 S.

C4- This conductor is located in the northernmost portion of the survey area and is stretching in the NE direction over a distance of 400 m approximately. Its estimated conductance is low and less than 5 S.

C5- This conductor is located in the northeast of the survey area, and northwest of the anomalous zone "An2". It is stretching in the EW direction roughly over a distance of less than 200 m, roughly. The estimated conductance is low and less than 5 S.

C6- This conductor is located in the southwest of the survey area, and southwest of the main anomalous zone "An1". It is stretching in the EW direction over a distance of 300 m approximately. The estimated conductance is low and less than 5 S.

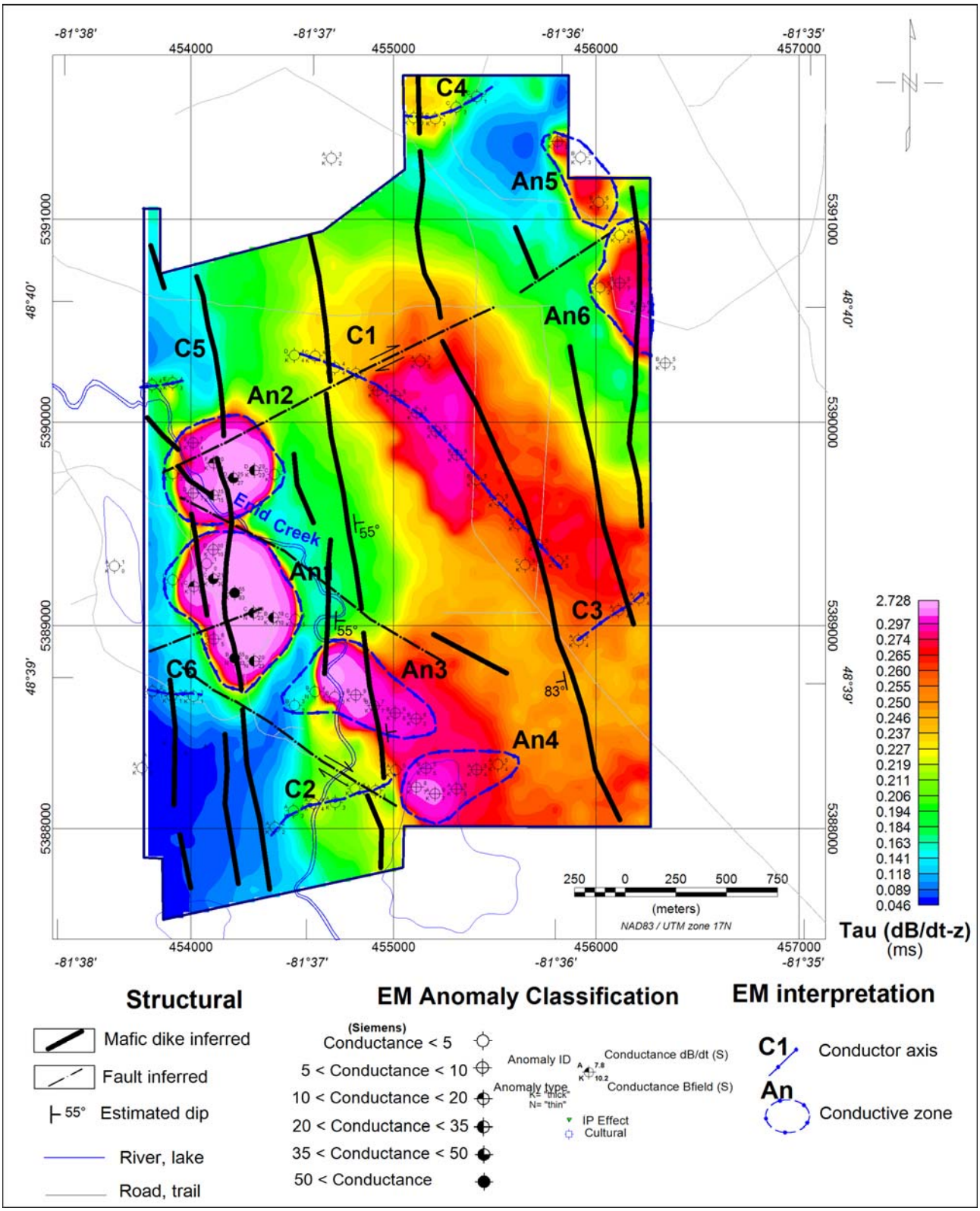

Figure 23: EM centres superimposed on the dB/dt-z time constant image.

7. INTEGRATED INTERPRETATION AND TARGETING RESULTS

7.1 GEOPHYSICAL RESPONSE OF NICKEL-SULPHIDE MINERALIZATION OF ENID CREEK

Ni-Cu-PGE sulphide mineralization within the survey area is hosted by a gabbroic intrusion. It is structurally controlled and occurs primarily at the gabbro/andesite contact, where the gabbroic intrusion has intruded into andesitic rocks. At depth, the gabbro is pyroxenitic, with potential for ultramafic composition at depth. Sulphide mineralization further occurs at or near the contact where the diabase dyke has cut into the gabbro, suggesting remobilization of the sulphides during contact. Sulphides also occur along fracture planes, but are limited to pyrite and/or marcasite. To date around fifty holes well drilled by various companies between 1957 and 2005. Nickel and copper mineralization has been intersected at various depths ranging from the near surface to a depth of up to 200 m, approximately.

Figures 24 to 26 show the historic drill holes plots with Ni, in red and Cu, in blue assays against the MVI, 1D conductivity and RDI models, respectively. From these Figures it's clear that Ni-Cu mineralization is associated with zones of elevated magnetization (from MVI inversion), elevated conductivity (from 1D inversion) and low resistivity (from RDI).

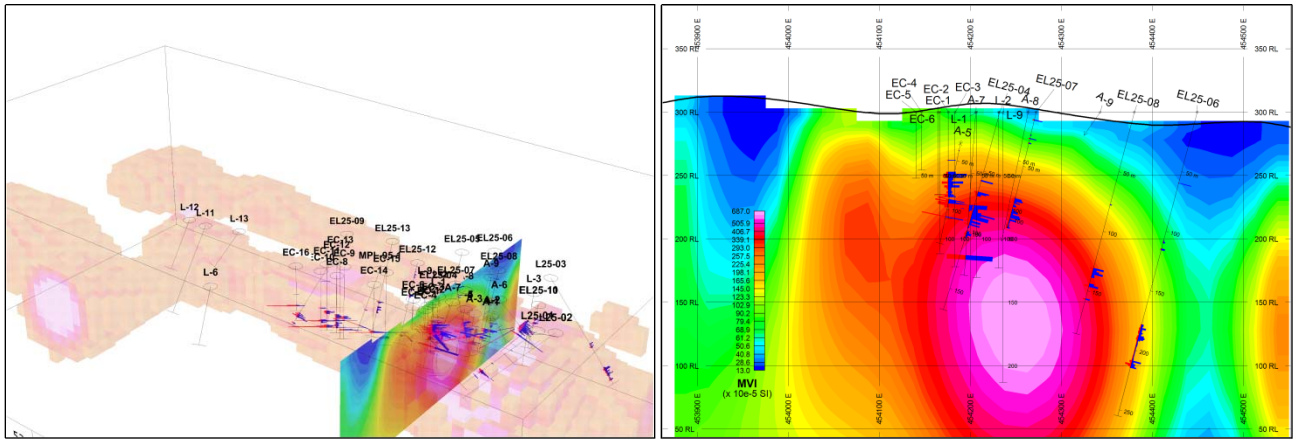

Figure 24: Left, drill holes with Ni (red) and Cu (blue) assays plotted with the MVI voxel with clipped lower magnetization values (>250×10^{-5} SI units), and right, MVI section with drill hole plots.

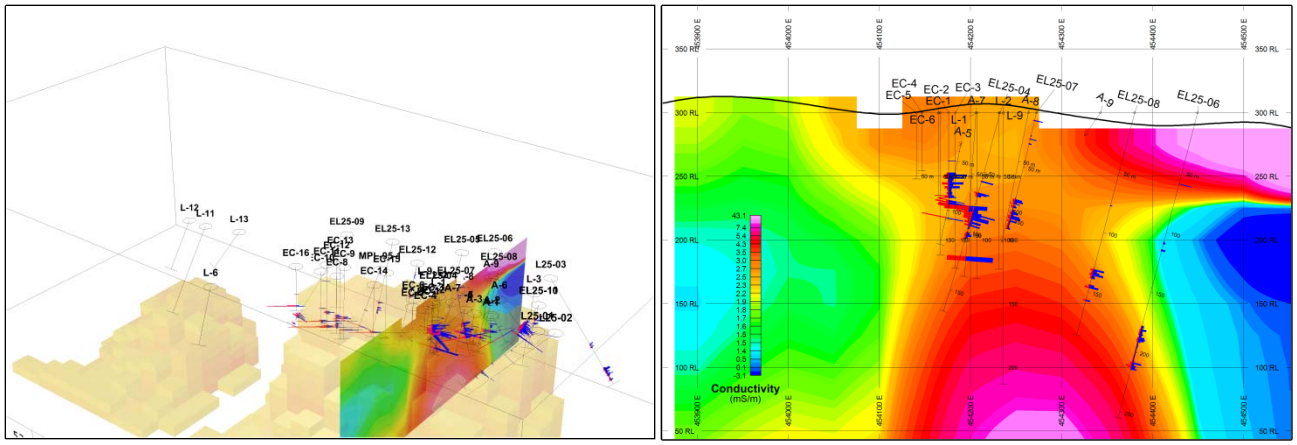

Figure 25: Left, drill holes with Ni (red) and Cu (blue) assays plotted with the 1D conductivity voxel with clipped lower conductivity values (>3 mS/m) and clipped top (elevation <230 m asl) and right, MVI section with drill hole plots.

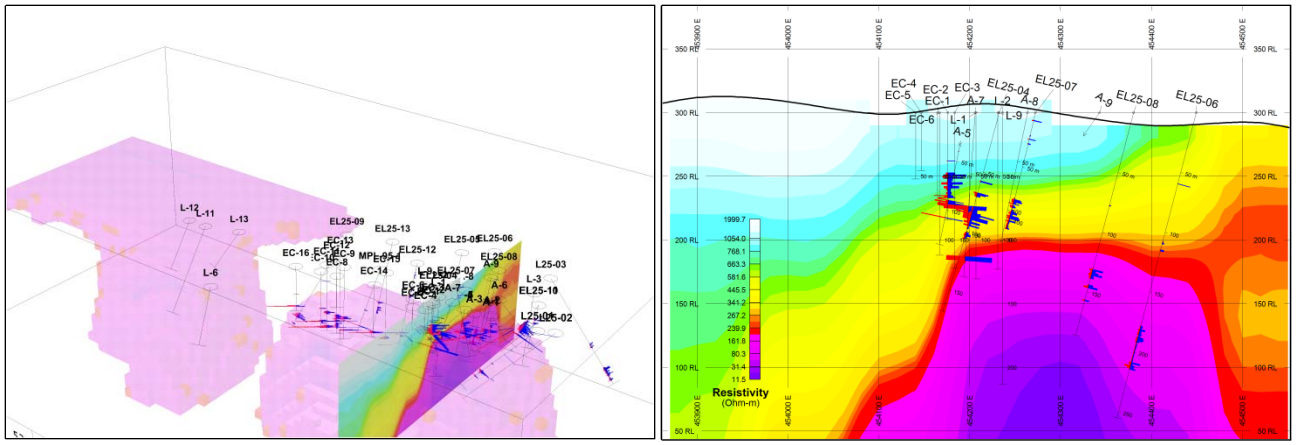

Figure 26: Left, drill holes with Ni (red) and Cu (blue) assays plotted against the RDI voxel with clipped higher resistivity values (<165 ohm-m) and clipped top (elevation <230 m asl) and right, RDI section with drill hole plots.

7.2 INTEGRATED INTERPRETATION MAP AND TARGET SELECTION

7.2.1 INTEGRATED MAP

Figure 27 presents an integrated interpretation map, which includes combined results from magnetic and VTEM data analysis and their inversion results. The magnetic interpretation results include the outlines of magnetic structures of mafic and ultramafic nature inferred from the 3D magnetic inversion, and inferred mafic dikes and faults. The VTEM interpretation results include the outlines of conductive zones as well as the plots of conductor axes inferred from VTEM data analysis. It also includes the outlines of VTEM targets inferred from 1D and 3D inversions.

From the structural point of view, the survey area includes rocks with various magnetic properties. Those exhibiting higher magnetization values are likely attributed to mafic and ultramafic rocks. They form small intrusions occurring along the inferred mafic dikes, which are striking in the NNW direction. Those with lower magnetization values are likely attributed to felsic volcanic and felsic intrusive rocks. This type of rocks is mostly encountered in the east part of the survey area. A number of magnetic dikes (dolerite or diabase) are highlighted from the magnetic interpretation. They cross-cut the entire survey area forming a dike system striking in the NNW direction at average azimuth of 10° NW. This dike system is cross-cut by fault structures striking in two preferred directions (NE 60° and NW 55°). These faults affect the dike system at their intersection causing horizontal offsets.

The VTEM interpretation and inversion results are suggesting the presence of six conductive zones and five linear conductors. The delineated conductive zones are mainly located in the west and the south of the survey area. They are characterized by various intensities. The most important anomalous zone is located in the west, south of Enid Creek and is associated with known nickel-sulphide mineralization. The rest of the zones are newly identified and remain however, untested. From the 1D and 3D inversion results, some conductive features are located at shallow depths (An1 and An3) and some others appear as deep-seated (An2, An4 and An6). The identified linear conductors are characterized by moderately low conductance and therefore, they are however, not considered as good targets for the exploration of massive nickel-sulphide mineralization. On the plan map, they are of various lengths and oriented in various directions.

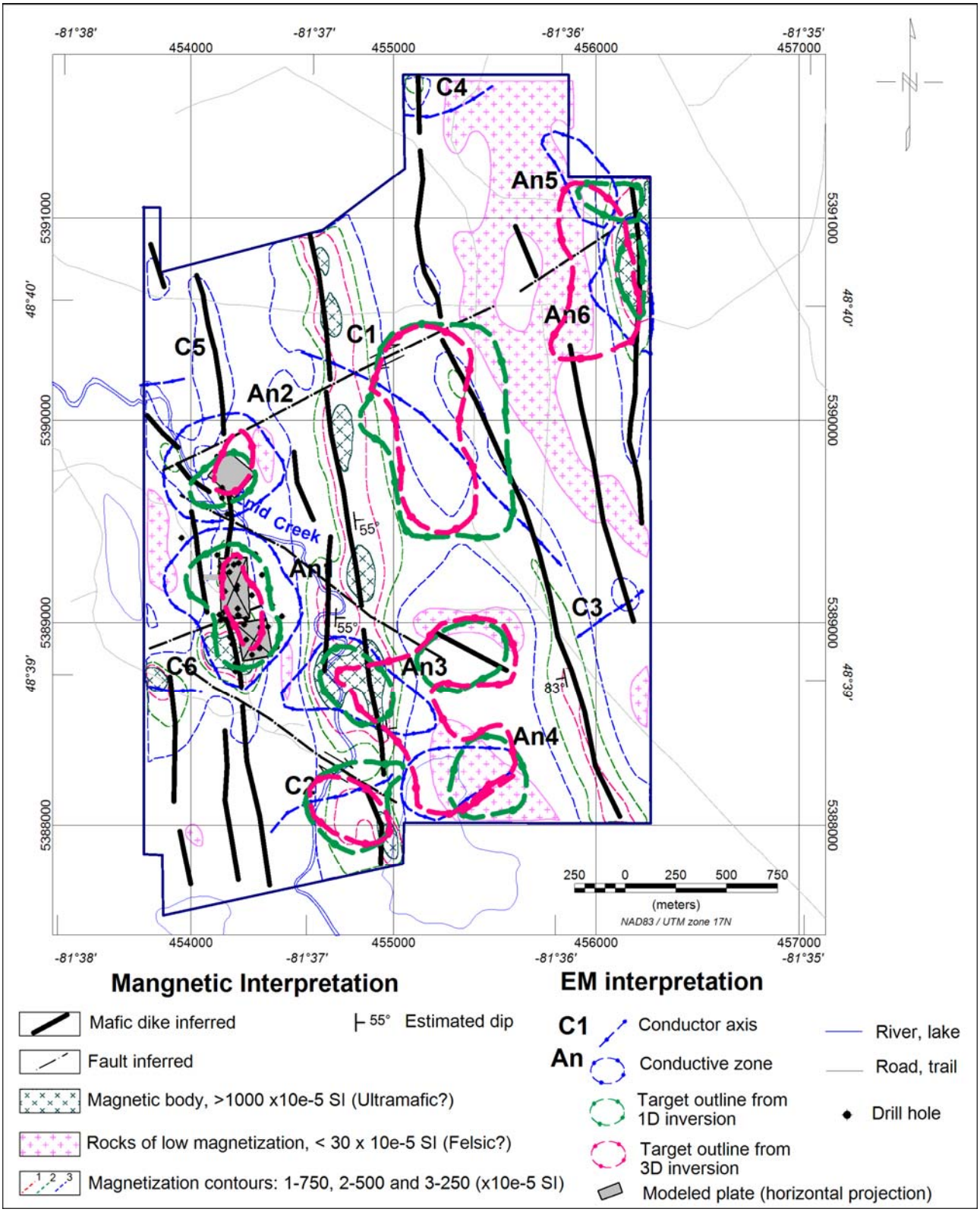

Figure 27: Integrated interpretation map of the study area including selected targets.

7.2.2 SELECTED TARGETS

Four 1st priority targets presenting a particular interest for the nickel-sulphide mineralization are selected for further detailed investigation and drill-testing. They are associated with conductive zones and magnetic zones. These targets are: An1, An2, An3 and An6. Additionally, two 2nd priority targets for nickel-sulphide mineralization are selected for further follow-up (C1 and C2). The latter appear as associated with deep-seated conductor axes occurring within zones of moderately elevated magnetization.

Targets An1 and An2

Target An1 is by far the most interesting one since it is associated with nickel-sulphide mineralization, intercepted by historic drill holes. From the modeling results the mineralization appears to be associated with a zone of conductivity high and a zone of elevated magnetization. From the 1D modeling results, the conductive zone appears to have further depth extent with the deeper part remaining untested. Target An2 was also drill tested with however, no mineralization intercepted. It is likely that this target is associated with deep-seated mineralization and therefore, deep holes would be recommended to test the deeper portion of this target.

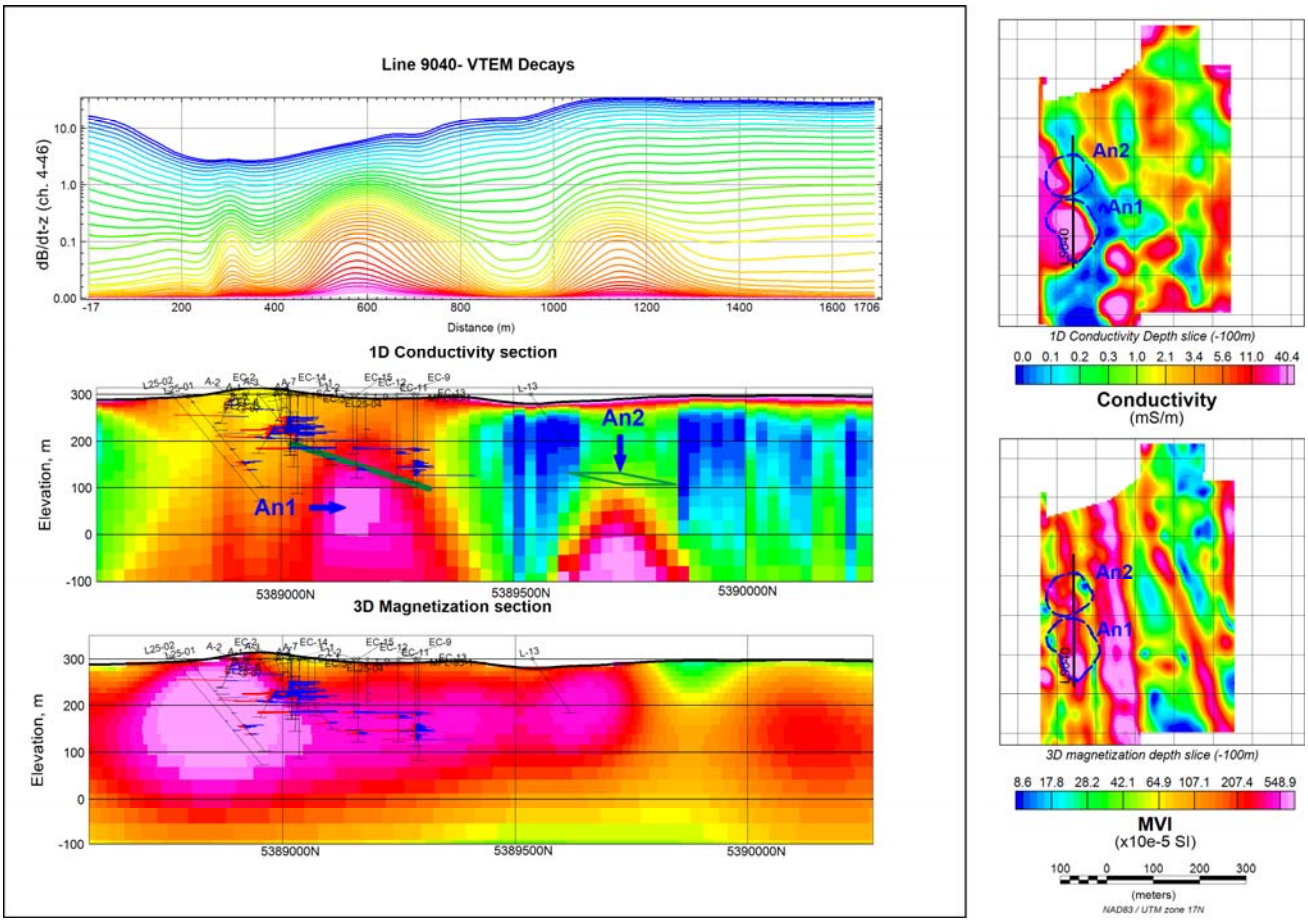

Figure 28: VTEM and magnetic modeling results for targets An1 and An2.

Targets An3

Target An3 is located southwest of Target An1 and exhibits similar EM response as target An2. It also occurs in association with a zone of elevated magnetization. From the 1D EM inversion results, the conductive source is suggested to be located at depth of 150 m approximately. However, the associated magnetic structure appears to be located at shallower depth (<100 m) as suggested from the 3D MVI inversion.

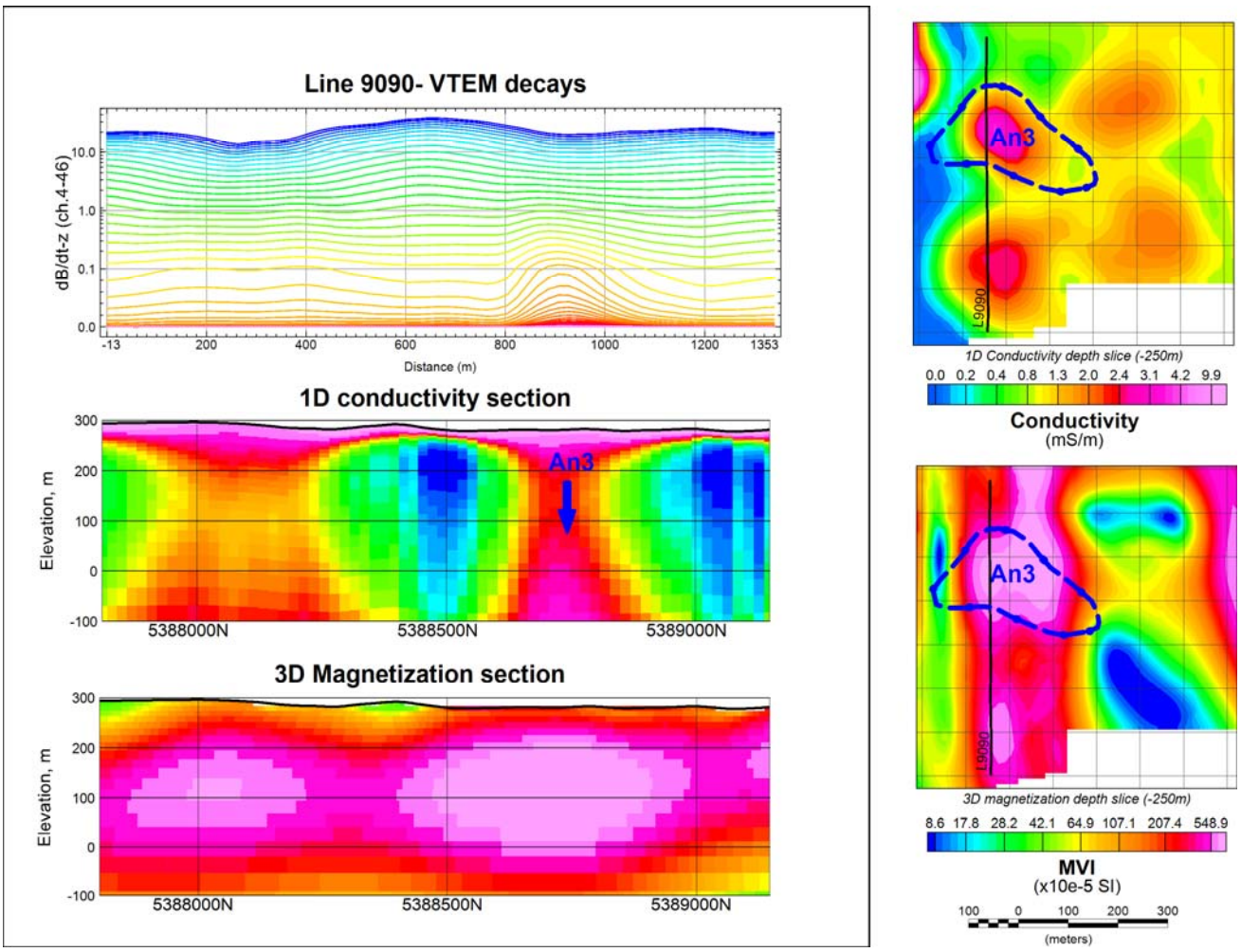

Figure 29: VTEM and magnetic modeling results for target An3.

Targets An6

This target is located in the northeast of the property. It is associated with a deep-seated (≈ 200m) conductive zone occurring in coincidence with a zone of elevated magnetization, whose top is located at depth of less than 100m.

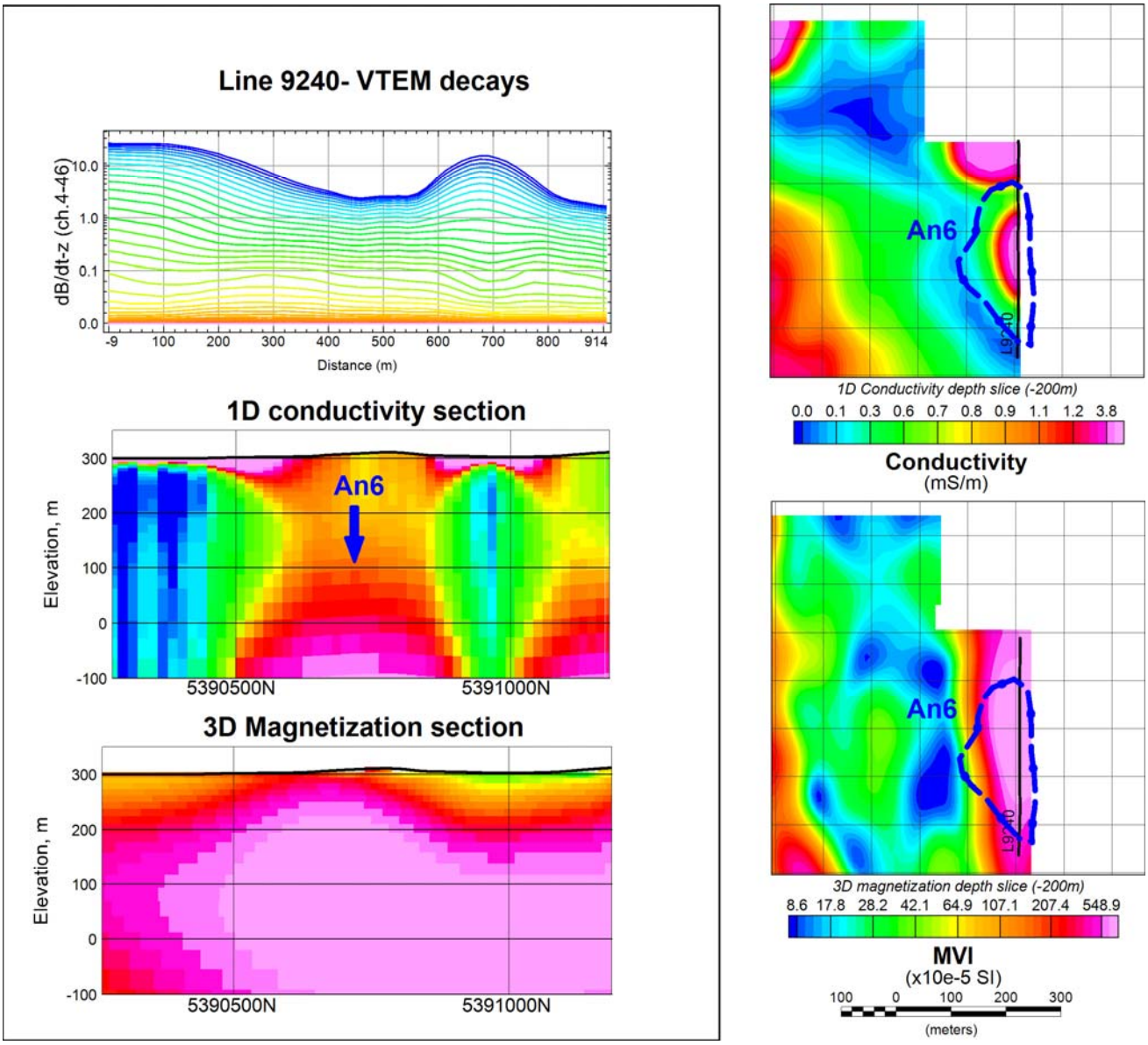

Figure 30: VTEM and magnetic modeling results for target An6.

Target C1:

Target C1 is located in the central area and appears as a linear conductor trending in the NW direction. From the 1D conductivity inversion results, the conductor appears as deep-seated (≈ 200m). It is associated with a zone of moderately elevated magnetization.

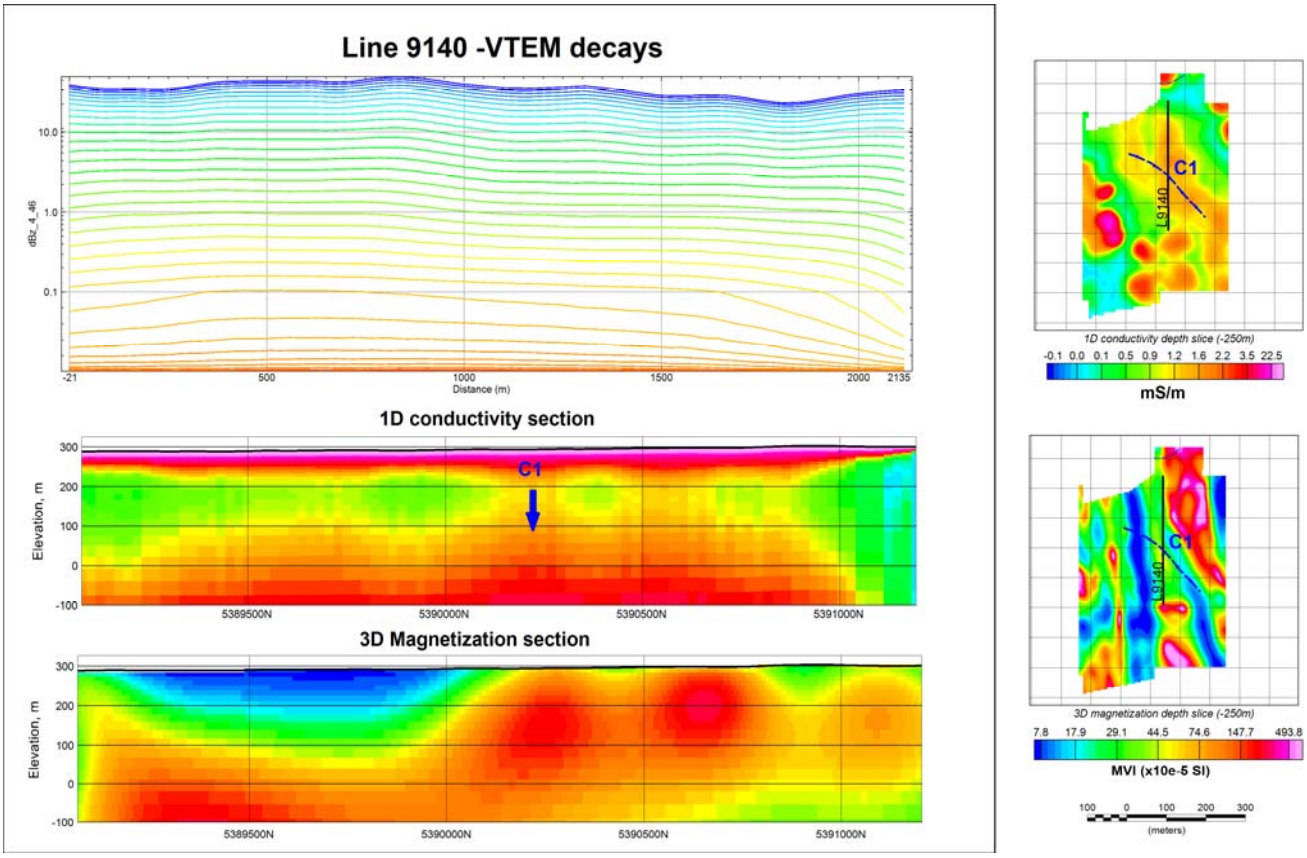

Figure 31: VTEM and magnetic modeling results for target C1.

Target C2:

Target C2 is located in the southern area south of the An3 anomalous zone. It appears as a linear conductor trending in the NE direction. From the 1D conductivity inversion results, the conductor appears as deep-seated (> 200m). It is associated with a zone of elevated magnetization.

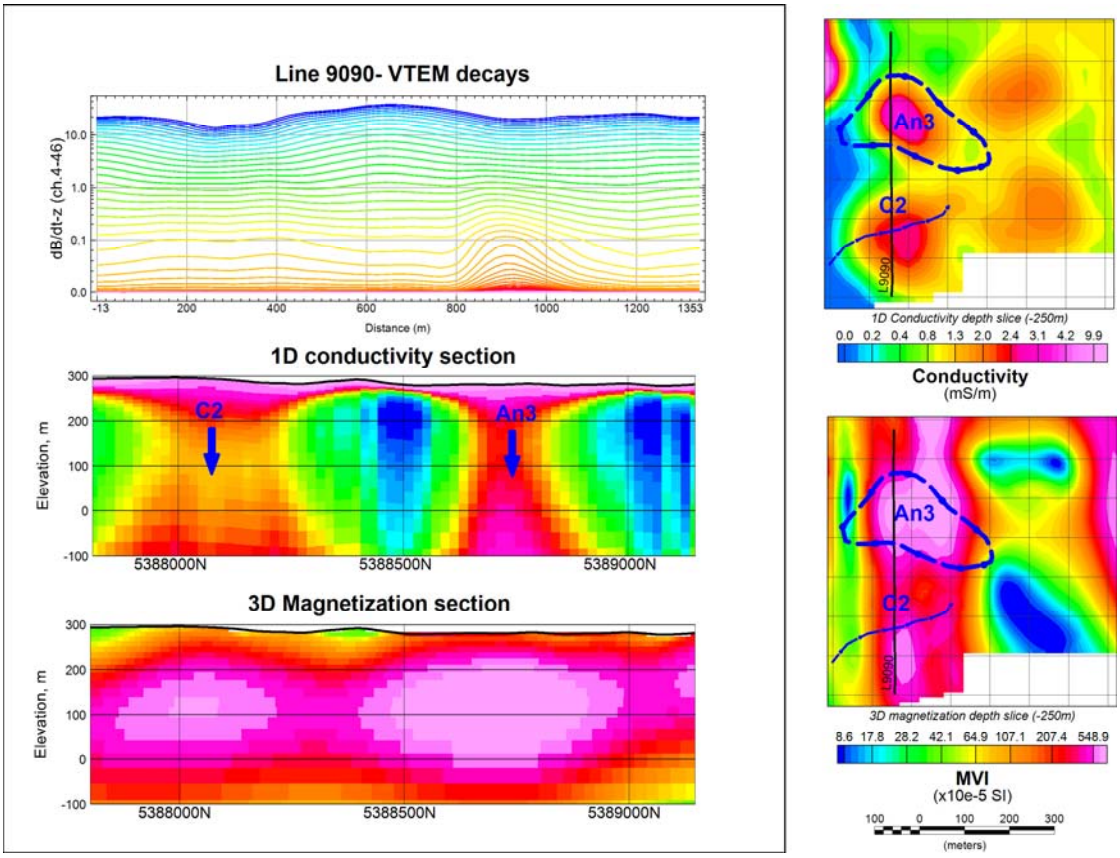

Figure 32: VTEM and magnetic modeling results for target C2.

8. CONCLUSIONS AND RECOMMENDATIONS

8.1 CONCLUSIONS

In the light of the interpretation and the inversion results of the VTEM and magnetic data acquired on the A Block, six (06) favourable targets areas presenting an interest for nickel-sulphide mineralization are delineated and selected for follow-up. Four (04) targets are associated with zones of elevated conductivity and elevated magnetization; these are considered as 1st priority targets. Two (02) targets associated with linear conductors exhibiting moderately elevated conductivity and occurring within zones of moderately elevated magnetization; these are considered are 2nd priority targets

8.2 RECOMMENDATIONS

The main recommendations for future follow-up work within the project area are summarized in the following points:

- Integrate the newly obtained results with all other available geological and geophysical information to prioritize exploration targets

- Drill test the identified targets based on the geophysical inversion results

Respectfully submitted

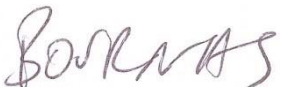

Nasreddine Bournas, P.Geo., PhD.
Senior Geophysicist
Geotech Ltd.

Alexander Prikhodko, P. Geo., PhD.
Director of Geophysics
Geotech Ltd.

July, 19th 2017

9. REFERENCES

- Annan, A. P., 1986, Development of the PROSPECT 1 airborne electromagnetic system, in Palacky, G. (ed), Airborne resistivity mapping: Geological Survey of Canada paper 86-22.

- Brodie R. C., 2015. GALEISBSTDEM: A deterministic algorithm for 1D sample by sample inversion of time-domain AEM data – theoretical details, Geoscience Australia

- Brodie R. C., 2016. User Manual for Geoscience Australia's Airborne Electromagnetic Inversion Software. Geoscience Australia.

- Duncan, A.C., 1987, Interpretation of down-hole transient EM data current filaments: Exploration Geophysics, 44, 6-15.

- Ellis, R.G., Barry de Wet, and I.N. Macleod, 2012. Inversion of Magnetic Data from Remanent and Induced Sources. ASEG Extended Abstracts 2012: 22nd Geophysical Conference:pp.1-4.

- Geological Map of Loveland and MacDiarmid Townships, Cochrane District. Scale 1:31,680 or 1 Inch to ½ Mile. Geology by R.S. Middleton and assistants, Geological Branch, 1970.

- Geotech, 2017, Report on a helicopter versatile time domain electromagnetic survey (VTEM™ max) and aeromagnetic geophysical survey on Block A, Halfmoon, Godfrey, Turnbull, Carscallen, Goose Egg, Wilky Walker and MontClerg: Timmins, Ontario FOR: International Explorers and prospectors Inc.. Technical report

- Gregory, S., 2007. Enid Creek PowerPoint Presentation; FNX presentation provided to Explores Alliance, 26 p.

- Legault, J. M., A. Prikhodko, D. J. Dodds, J. C. Macnae, G.A. Oldenborger, 2012, Results of recent VTEM helicopter system development testing over the Spiritwood Valley aquifer, Manitoba: 25TH SAGEEP Symposium on the Application of Geophysics to Engineering and Environmental Problems, Expanded Abstract, 17p.

- Li, Y. and Oldenburg, D.W., 1996. 3D inversion of magnetic data: Geophysics, vol. 61, no. 2, p.394-408.

- Macnae, J., and Baron-Hay, S., 2010, Reprocessing strategy to obtain quantitative early-time data from historic VTEM surveys, Expanded abstract, 21ST International Geophysical Conference & Exhibition, ASEG, 5 pp.

- Meju M.A., 1998, A simple method of transient electromagnetic data analysis. Geophysics, 53 (2)- 405-410.

- Prikhodko, A. Morrison, E. Bagrianski, A. Kuzmin, P. Tishin, P. and Legault, J., 2010, Evolution of VTEM-Technical solutions for effective exploration.21st ASEG conference and Exhibition, Expanded Abstracts, 1-4.

- Schaa, R., and P.K. Fullagar, 2012, Vertical and Horizontal resistive limit formulas for rectangular-loop source on a conductive half space.E91-E99 Geophysics, 77(1), E91-E99.

- Vanderklift,W., Van Luven C., and Voormeij, D. A.,2005, Report on Enid Creek Property, Loveland Township, Ontario.

- Witherly, K., R. Irvine, and E. B. Morrison, 2004, The Geotech VTEM time domain helicopter EM system, SEG, Expanded Abstract, 1217-1221.

Appendix A

Coordinates of selected target-areas
Coordinates are in meters (NAD 83/UTM Zone 17N projection)

A- 1st Priority targets

An1

Corner	Easting, m	Northing, m
1	454104.9	5389321
2	454282.1	5389362
3	454426.1	5388836
4	454260.0	5388797

An2

Corner	Easting, m	Northing, m
1	454176.9	5389960
2	454354.1	5389908
3	454232.3	5389578
4	454063.4	5389656

An3

Corner	Easting, m	Northing, m
1	454884	5388474
2	455077.9	5388681
3	454741.8	5388948
4	454575.9	5388737

An6

Corner	Easting, m	Northing, m
1	456267.0	5391012
2	456055.9	5391005
3	456062.3	5390451
4	456262.7	5390454

B- 2nd Priority targets

C1

Corner	Easting, m	Northing, m
1	454933.5	5390441
2	454931.4	5389637
3	455304.1	5389435
4	455420.4	5390307

C2

Corner	Easting, m	Northing, m
1	454713.3	5387888
2	455064.2	5388002
3	454756.3	5388385
4	454491.3	5388249

Appendix B

EM anomaly listing
(Also provided in Excel and Geosoft database)

Line ID	X, m	Y, m	Zb, m	Radarb, m	DEM, m	Anom. Type (*)	Anom. Label	Anom. Cond (dB/dt), S	Anom. Cond. (BField), S	IP effect
9000	453812.2	5388345	342.3	48.2	290.9		A			1
9000	453810	5388676	349.4	50.9	295.3	K	B	1.8	0.6	
9000	453807.7	5390185	346.9	60.0	283.7	K	C	3.7	1.9	
9010	453907.2	5388405	341.4	48.9	289.3		A			1
9010	453906.4	5388654	350.4	52.6	294.5	K	B	2.4	1.0	
9010	453910.4	5389225	368.7	51.8	313.6	K	C	3.0	1.1	
9010	453910.8	5389747	346.9	45.3	298.4	K	D	4.1	1.6	
9010	453909.9	5390195	350.4	50.4	296.8	K	E	3.8	2.7	
9020	454012.8	5388353	341.2	48.7	289.3		A			1
9020	454012.3	5388651	351.4	51.0	297.1	K	B	2.6	1.1	
9020	454014.4	5389192	355.2	55.0	297.0	K	C	12.1	10.4	
9020	454011.2	5389651	355.3	61.4	290.7	K	D	8.5	6.7	
9020	454010.9	5389900	351.3	52.0	296.0	K	E	7.3	3.8	
9030	454107.8	5388386	338.2	45.7	289.2		A			1
9030	454113.3	5388933	353.9	50.3	300.4	K	B	6.2	4.6	
9030	454110.7	5389230	346.4	50.9	292.3	K	C	21.2	29.8	
9030	454110.4	5389374	349.2	54.2	291.7	K	D	9.7	9.9	
9030	454111.9	5389642	347.3	57.5	286.5	K	E	15.2	15.3	
9030	454112.5	5389800	345.6	49.5	292.9	K	F	10.0	11.2	
9040	454212.9	5388297	340.0	49.0	287.8		A			1
9040	454215.6	5388839	355.4	52.5	299.6	N	B	55.5	82.8	
9040	454215.9	5389161	352.6	57.0	292.3	K	C	55.5	82.8	
9040	454209.5	5389726	341.5	48.5	289.8	K	D	25.2	26.6	
9050	454312.2	5388371	337.1	48.4	285.4		A			1
9050	454312.7	5388824	343.5	50.6	289.7	N	B	19.6	23.2	
9050	454309.4	5389062	347.7	49.9	294.5	N	C	19.6	23.2	
9050	454313.9	5389764	346.8	49.5	294.1	K	D	19.6	23.2	
9060	454414.6	5388007	330.3	44.5	282.6	K	A	2.2	1.8	1
9060	454407.7	5389039	334.6	41.5	289.8	K	B	17.6	110.2	
9060	454412.6	5389744	345.3	50.0	292.0	K	C	3.8	3.1	
9070	454506.6	5388088	339.6	46.1	290.2	K	A	3.5	2.7	
9070	454511.7	5388607	339.3	50.0	286.1	K	B	2.6	1.9	
9070	454514.8	5389030	343.0	47.5	292.3	K	C	4.9	4.7	
9070	454510.4	5390331	348.6	50.7	294.7	K	D	4.0	3.6	
9080	454606.5	5388123	337.4	54.7	279.5	K	A	4.1	3.6	
9080	454612.7	5388674	343.4	51.8	288.4	N	B	4.1	3.6	
9080	454613.1	5390328	352.5	54.0	295.3	K	C	4.3	3.7	
9090	454712.2	5388128	335.0	41.6	290.1	K	A	3.9	3.3	
9090	454709.5	5388648	335.3	50.9	281.1	N	B	3.9	3.3	
9090	454710.6	5390270	339.6	42.7	293.7	K	C	4.2	4.0	
9100	454809.9	5388197	349.0	50.5	295.3	K	A	4.0	3.7	
9100	454814	5388658	349.7	49.6	296.9	K	B	9.1	9.5	
9100	454814.5	5390240	342.0	46.9	292.0	K	C	4.4	4.1	
9110	454911.8	5388187	344.6	45.6	295.8	K	A	4.2	3.6	
9110	454904.2	5388605	346.5	46.2	297.1	K	B	7.0	6.8	
9110	454921.6	5390157	337.4	41.9	292.3	K	C	5.1	4.3	
9120	455010.2	5388289	341.5	45.5	292.8	K	A	4.8	4.3	

9120	455009.3	5388570	345.7	48.8	293.7	K	B	6.4	5.5	
9120	455009.1	5390132	343.7	48.3	292.2	K	C	5.2	4.3	
9130	455112.1	5388204	344.3	52.9	288.1	K	A	8.2	6.8	
9130	455111.3	5388541	341.5	48.2	290.1	K	B	5.8	5.0	
9130	455114.2	5390047	344.4	48.0	293.2	K	C	5.4	4.4	
9130	455099.3	5391500	351.4	45.1	303.1	K	D	4.1	3.3	
9140	455204.6	5388172	337.5	48.0	286.2	K	A	8.6	6.8	
9140	455210.4	5389956	338.1	43.1	291.8	K	B	5.5	4.6	
9140	455206.2	5391494	353.2	48.8	301.2	K	C	4.2	3.3	
9150	455311.1	5388196	346.5	55.3	287.9	K	A	5.4	5.2	
9150	455312.7	5389839	341.8	46.5	292.1	K	B	5.6	4.6	
9150	455309.8	5391552	353.1	49.1	300.8	K	C	4.0	2.5	
9160	455410.1	5388290	346.6	50.1	293.2	K	A	5.2	4.4	
9160	455408.8	5389717	343.1	47.7	292.1	K	B	4.9	4.5	
9160	455409.8	5391604	351.7	47.3	301.1	K	C	3.1	0.9	
9170	455514.3	5388317	342.1	43.5	295.3	K	A	4.8	4.2	
9170	455516	5389617	342.4	47.2	292.0	K	B	4.9	4.5	
9180	455613.7	5389500	341.3	47.4	290.6	K	A	4.9	4.5	
9190	455712.9	5389400	343.3	50.2	289.8	K	A	5.0	4.7	
9200	455810.9	5389318	338.5	45.1	290.2	K	A	4.9	4.7	
9200	455808.8	5391383	348.4	46.0	299.1	K	B	5.2	1.7	
9210	455911.9	5388928	343.3	51.1	289.0	K	A	4.7	4.3	
9220	456018.5	5390665	352.6	47.0	302.3	K	A	4.6	1.7	
9220	456011.6	5391084	354.9	48.0	303.7	K	B	4.7	3.0	
9230	456110.4	5389073	346.3	49.8	293.2	K	A	4.9	4.2	
9230	456116.4	5390687	353.2	46.6	303.4	K	B	5.3	3.5	
9230	456116.6	5390922	354.5	48.8	302.4	K	C	4.2	1.9	1
9240	456211.8	5389135	345.4	47.4	294.8	K	A	4.8	4.1	
9240	456214.6	5390570	358.0	52.1	302.6	K	B	5.8	3.9	
9240	456214	5390964	358.0	51.7	303.1	K	C	4.2	1.2	1
10000	454693.3	5391300	350.3	49.0	298.1	K	A	2.8	2.3	
10000	455923.2	5391305	360.7	55.0	302.5	K	B	4.9	3.1	
10010	455131.4	5390302	340.2	43.4	293.5	K	A	4.8	4.6	
10010	456340.4	5390292	351.9	46.1	302.6	K	B	5.2	3.0	
10020	453622.8	5389293	358.4	61.5	293.7	K	A	0.5	0.5	1
10020	454077.7	5389306	355.7	63.4	289.0	N	B	0.5	0.5	
10020	455649.1	5389300	343.2	49.7	290.3	K	C	4.7	4.3	
10030	453759	5388299	333.1	41.0	288.9	K	A	0.6	0.5	1
10030	455160.4	5388297	339.4	49.5	286.7	K	B	5.3	4.9	

(*) K- Single peak anomaly
N-Double peak anomaly

Appendix C

MVI Sections
(Provided in a separate PDF file)

Appendix D

MVI Depth Slices
(Provided in a separate PDF file)

Appendix E

Magnetic susceptibility Sections
(Provided in a separate PDF file)

Appendix F

Magnetic susceptibility Depth Slices
(Provided in a separate PDF file)

Appendix G

1D Conductivity Sections
(Provided in a separate PDF file)

Appendix H

1D Conductivity Depth Slices
(Provided in a separate PDF file)

Appendix I

RDI Sections
(Provided in a separate PDF file)

Appendix J

RDI Depth Slices
(Provided in a separate PDF file)

Appendix K

VTEM 2.5 D inversion results
(EMIT Maxwell Plate algorithm)
(Provided in a separate PDF file)